Journal of Paleolithic Archaeology (2023) 6:34
https://doi.org/10.1007/s41982-023-00160-0

RESEARCH

A Context for Connectivity: Insights to Environmental Heterogeneity in the Late Pleistocene and Holocene of Southern Africa Through Measuring Isotope Space and Overlap

Joshua R. Robinson

Accepted: 14 September 2023

Abstract

Southern Africa is characterized by the development of varied Middle and Later Stone Age techno-complexes and behaviors against a backdrop of complex climatic conditions during the late Pleistocene and Holocene. While much work has been devoted to reconstructing regional environmental patterns, site-specific ecological and habitat contexts have primarily focused on a single site or small area. The local manifestations of regional climatic conditions are analyzed here by compiling faunal enamel stable isotope data from 13 sites across South Africa, Lesotho, and Zambia. Measuring isotope space and overlap reveals distinct on-the-ground habitat circumstances across regions and even variability within some regions, especially in the period ~ 36,000–5000 years ago. This analytical framework aims to test whether sites within the same environmental zones overlap in isotope space and finds that there is greater intra-regional environmental heterogeneity than expected. Patterns of contracting and expanding isotope space, especially along the oxygen axis, may provide insight to shifts in rainfall seasonality and, perhaps, sources of precipitation. This increased understanding of the local manifestations of regional climatic conditions through time and space will be a critical component of models of population movement and interactions in the late Pleistocene and Holocene of southern Africa.

Keywords Stable isotopes · Southern Africa · Middle Stone Age · Later Stone Age · C_3 grasses · Winter rainfall

✉ Joshua R. Robinson
joshrobi@bu.edu

Published online: 08 November 2023

Introduction

Recognition of the pan-African nature of human evolution (e.g., Hublin et al., 2017; Scerri et al., 2018, 2019) has led to a consideration of archaeological sites as parts of interconnected landscapes (e.g., Mackay et al., 2014; Stewart & Mitchell, 2018). As seen in a recent model of "Out of Africa" migration scenarios (Beyer et al., 2021), regional and local climatic contexts are a crucial component in determining which dispersal corridors for human populations would have been climatically feasible at different time periods. Therefore, our understanding of the connectivity of Middle Stone Age and Later Stone Age (MSA and LSA, respectively) networks in southern Africa requires also thinking of environmental and habitat data as part of these broader landscapes. While much work has been geared towards constructing drivers of regional climatic conditions from off-shore or terrestrial datasets disconnected from the archaeological record (e.g., Chase, 2021; Dupont et al., 2022; Quick et al., 2016), there has generally been less focus on building regional paleoenvironmental reconstructions from the ground up based on the local resolution of proxies combined from multiple sites (although see Stratford et al., 2021, and papers therein). In line with the theme of this special issue (Val & Collins, 2022), I aim to synthesize the record of faunal enamel carbon and oxygen stable isotope data ($\delta^{13}C_{enamel}$ and $\delta^{18}O_{enamel}$, respectively) from late Pleistocene and Holocene sites across the broader southern Africa region in order to move beyond individual sites and begin interpreting regional spatial and temporal variation in southern African environments.

Working with such a large dataset offers the opportunity to apply novel analytical techniques to identifying and interpreting isotope patterns in addition to traditional methods of statistical comparison. Here, isotope space analyses (sometimes referred to as isotope niche space), including space occupied and space overlapped, are calculated. Isotope space measures have been used in ecology for nearly two decades (Eckrich et al., 2020; Jackson et al., 2011; Newsome et al., 2007) and have recently been directly applied to paleoanthropological and archaeological cases (Baumann et al., 2023; Hermes et al., 2018; Lüdecke et al., 2022; Robinson, 2022). Unlike traditional comparative statistics, isotope space analyses offer the ability to consider isotopes of different elements, in this case $\delta^{13}C_{enamel}$ and $\delta^{18}O_{enamel}$, at once in a single measure. Moving beyond a simple bi-plot with one element mapped on the *x*-axis and one on the *y*-axis, this approach uses spatial statistics to calculate the total amount of space occupied by a study group (i.e., an archaeological site) on the plot and the degree of spatial overlap among groups plotted on the same chart. Thus, quantification of isotope space and isotope space overlap allows for testing hypotheses about the similarities and differences among groups that qualitative comparisons of bi-plots and/or descriptive statistics (mean and standard deviation) cannot assess alone. This approach has a particular value when multiple archaeological sites are being compared and considered, as will be done in this study, and the specific details of how isotope space measures are calculated here are described further in the Materials and Methods.

Environmental Context

The paleoenvironmental record and climatic variations of southern Africa over the last ~ 100,000 years are challenging to interpret. Attempts to synthesize site-level environmental datasets into regional reconstructions have a long history in southern Africa (Deacon, 1983; Deacon & Lancaster, 1988). Recent efforts to apply multi-site local environmental records to interpreting variations in a regional climate include a focus on the winter rainfall zone (Chase & Meadows, 2007) and coastal southern Africa more broadly (Carr et al., 2016). Paleoenvironmental research in southern Africa has also trended to multi-proxy analyses of individual sites (e.g., Ames et al., 2020; Chazan et al., 2020; Lukich et al., 2020) and/or smaller regions, such as the Paleo-Agulhas Plain (PAP; Marean et al., 2020 and related papers therein). A comprehensive review of southern African climates is beyond the scope of the current contribution, but as I follow the more inclusive characterization of southern Africa provided by Val & Collins (2022), here I offer a brief synopsis of the intra-regional environmental dynamics as context for the site-level stable isotope compilation.

Environments in the western, eastern, and interior sections of southern Africa are influenced by different climatic and ecological drivers and may have even been climatically decoupled at times in the late Pleistocene and Holocene (Chase, 2021; Chase et al., 2021; Dupont et al., 2022; Knight & Fitchett, 2021). It is thought that the diversity of rainfall sources and regimes that influence the region today was generally the same over the last ~ 150,000 years (Carr et al., 2016; Chase & Meadows, 2007). In the western section of the region, this includes the winter rainfall zone (WRZ) that grades into a year-round rainfall zone (YRZ) across parts of Namibia and the interior and the southern coast of South Africa and, finally, into a summer rainfall zone (SRZ) somewhere north of modern-day Port Elizabeth (Fig. 1; Carr et al., 2016; Chase & Meadows, 2007). While much of southern Africa has summer rainfall due to the southward migration of the Intertropical Convergence Zone (ITCZ), the complex interplay of Atlantic and Indian Ocean air masses and the expansion of the circumpolar vortex in the winter cause westerly cyclonic systems to bring rain to the WRZ of the southwestern Cape and parts of the YRZ (Chase & Meadows, 2007; Chase et al., 2013, 2017; Tyson & Preston-Whyte, 2000; van Zinderen Bakker, 1976). There is a statistical antiphase relationship between rainfall patterns in the SRZ and WRZ, meaning that sites across these regions can be correlated to show broadly coeval responses to climate forcing (Carr et al., 2016; Chase et al., 2017; Roffe et al., 2021). Precipitation patterns in the YRZ are complicated further by the influence of the Agulhas Current which at times may have brought more tropical climate signals to the southern Africa coast (Chase & Quick, 2018).

Recently, Chase (2021) has demonstrated that precipitation in southeastern Africa is controlled by changes in the seasonality of insolation as a result of eccentricity and precession. Periods of higher eccentricity are associated with increased rainfall and more humid conditions while reduced eccentricity and higher global ice volume are associated with drier conditions in southern Africa overall. Along the southeastern Africa coast, precipitation patterns broadly follow the expansion and contraction cycles of the SRZ and WRZ, with greater summer rain associated with more rainfall over southern Africa overall (Chase, 2021). While Northern Hemisphere cooling

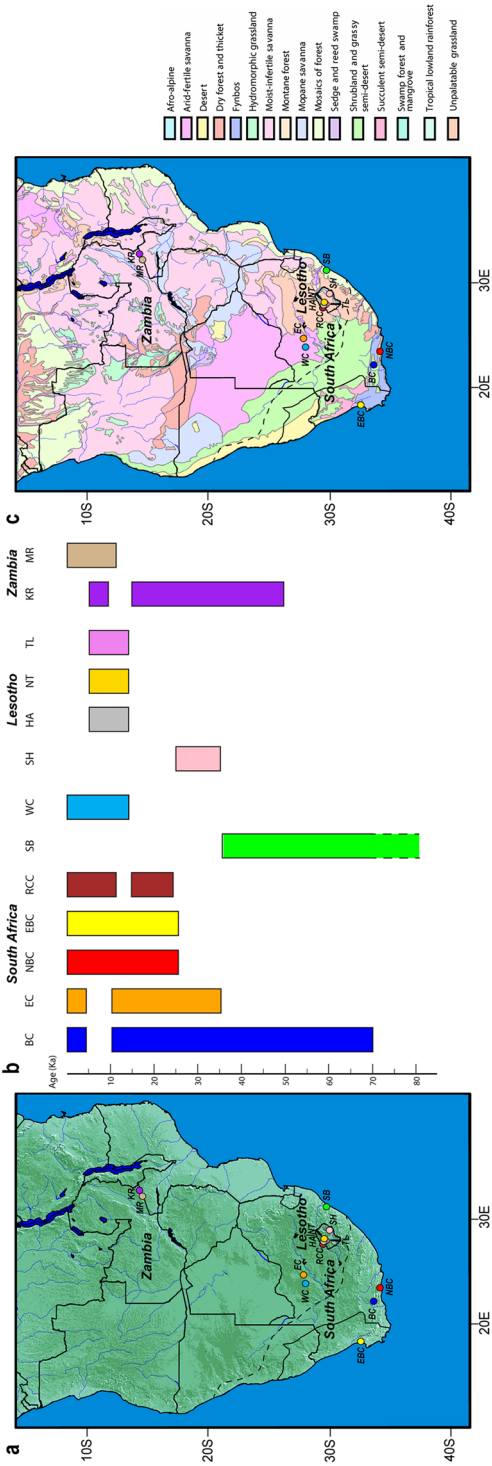

Fig. 1 Map of southern Africa indicating the locations of the study sites (**a**) and the approximate extent of the winter rainfall zone (WRZ) with a solid line and the summer rainfall zone (SRZ) with a dashed line following Chase & Meadows (2007). **b** Chronology of layers/units from which stable isotope samples are available from the study sites. BC, Boomplaas Cave; EC, Equus Cave; NBC, Nelson Bay Cave; EBC, Elands Bay Cave; RCC, Rose Cottage Cave; SB, Sibhudu; WC, Wonderwerk Cave; SH, Sehonghong; HA, Ha Makotoko; NT, Ntloana Tsoana; TL, Tloutle; KR, Kalemba Rockshelter; MR, Makwe Rockshelter. Stratigraphic sections based on Mitchell (1993a, 1993b), Smith et al. (2002), Mitchell & Vogel (1994), Loftus et al., (2015, 2016, 2019), Pargeter et al., (2017, 2018), Miller et al. (1999), Vogel (2001), Sealy et al., (2016, 2020), Stowe & Sealy (2016), Beaumont et al. (1992), Lee-Thorp & Beaumont (1995), Wadley (1995), Jacobs et al., (2008a, 2008b), Ecker et al., (2017, 2018), Rhodes et al. (2022), and Phillipson (1973, 1976). **c** Map of simplified vegetation zones following White (1983). Assigned abbreviations and colors used throughout the figures

and glaciation resulted in overall wetter conditions for coastal southern Africa during the Last Glacial Maximum (LGM), Engelbrecht et al. (2019) projected the eastern coastal regions of southern Africa to have lower rainfall totals. At the same time, climatic conditions further north to the Zambezi Basin would have been wetter as the result of an equatorward shift of winter frontal rainfall (Chase, 2021; Engelbrecht et al., 2019).

Related to Quaternary climatic and vegetation trends along the southern African coast is also a need to consider the role of landscape change, particularly the expansion of the Agulhas Plain due to lower sea levels during the middle and late Pleistocene (Cawthra et al., 2020; Fisher et al., 2010; Marean et al., 2020). Sea level change during the LGM has been modeled to be a maximum of 125–130 m lower than the present, but even smaller changes would have exposed significant areas of land that are today under water. Global climate changes in conjunction with extended coastlines have often been associated with increased interior aridity in southern Africa that may have prevented extensive human activity in the region (Blome et al., 2012; Carr et al., 2016; Chase, 2009, 2010; Thomas & Burrough, 2012, 2016), although there is recent evidence that human populations successfully occupied these interior environs in the long term (Bousman & Brink, 2018; Knight & Stratford, 2020; Stewart & Mitchell, 2018; Wilkins, 2021), with human populations supported by large-scale, now-dry paleolakes (Carr et al., 2023).

The preceding discussion makes clear that the southern African climatic record of the late Pleistocene and Holocene is highly variable from region to region and difficult to disentangle at present based on current proxy evidence. Great strides have been made in deciphering the role of climatic forcing mechanisms on precipitation patterns (Chase, 2021; Chase et al., 2013, 2021; Engelbrecht et al., 2019) and vegetation regimes (Dupont et al., 2022; Quick et al., 2016), as well as resurrecting the lost PAP ecosystem (Marean et al., 2020). The current study acknowledges the complexity of fitting together and spatiotemporally nesting local and regional environmental and habitat conditions. With this in mind, I apply an explicitly hierarchical framework to test the relationship between local environmental data, in the form of $\delta^{13}C_{enamel}$ and $\delta^{18}O_{enamel}$ records from individual late Pleistocene and Holocene archaeological sites, and the regional climatic models of this period described earlier in southern Africa. Establishing how regional conditions manifest locally at individual sites will allow for more nuanced approaches to investigating human mobility and connectivity during the MSA and LSA. Many exciting recent studies rely on lithic materials (Schoville et al., 2022; Way et al., 2022) and ostrich eggshell beads (Stewart et al., 2020) in building models of movement and/or social networks at different points in the late Pleistocene of southern Africa. A locally informed reconstruction of paleoenvironments across the region could be paired with these models to explore questions about timing, directionality, and the relative influence of environmental and social factors on human mobility and behavioral exchange. For example, Mackay and colleagues' (2022) investigation of novel behaviors at Varsche River 003 suggests innovation and cultural transmission being environmentally contingent processes during the MSA.

Archaeological Background and Study Sites

A rich and diverse record of material culture spanning the last ~ 100,000 years has been recovered from southern African archaeological sites with local differences in the timing and transition of regionally recognized techno-complexes (e.g., Wadley, 2015; Wilkins, 2021; Yandel et al., 2016). While attempts have been made to directly connect changes in techno-complexes and other material cultures of the southern African record to climatic and environmental factors (e.g., Backwell et al., 2014; McCall, 2007; Ziegler et al., 2013), the occurrence of diagnostic assemblages like the Still Bay and Howiesons Poort across diverse habitats seems to suggest that technological transitions are largely independent of environmental conditions (Jacobs & Roberts, 2009). Furthermore, local environmental reconstructions at sites like Sibhudu have failed to identify major changes in habitats or climatic conditions between technological periods (Robinson & Wadley, 2018; although see Nel & Henshilwood, 2016, for a possible counterargument at Blombos). It is likely that demographic factors and responses to regional and local environmental events combined in complex ways in the development of southern African techno-complexes and material culture patterns (Mackay et al., 2014; Sealy, 2016). As such, it is not the goal to correlate transitions in material culture, at either individual sites or regional techno-complexes, to changing environmental conditions identified locally. Instead, this study compiles $\delta^{13}C_{enamel}$ and $\delta^{18}O_{enamel}$ data in order to create a multi-site database for testing hypotheses about southern African paleoenvironments in the late Pleistocene and Holocene.

Stratford et al. (2021) identify 104 cave and rockshelter sites in southern Africa with sediments dating to the last ~ 100,000 years. Added to this is a number of open-air sites, especially those in the Kalahari Basin (e.g., Wilkins, 2021). Out of all of these sites, Stratford et al., (2021: 902) show that only 5% of cave and rockshelter sites in southern Africa have stable isotope analyses on bone or tooth enamel published. No faunal stable isotope data are published for any of the interior open-air sites, although part of the reason for this is a lack of preservation of faunal remains at open-air and other interior sites. While stable isotope data from bone and "tooth collagen" of dentine have been published for Apollo 11 Cave in Namibia and Melikane Cave in Lesotho (Vogel, 1983), the preservation of collagen at these time periods is dubious and a lack of published C:N ratios makes it difficult to assess the reliability of these results (e.g., France & Owsley, 2015). As such, only stable isotope analyses conducted on tooth enamel are considered here.

Stable isotope data from faunal tooth enamel have been published from late Pleistocene and early mid-Holocene contexts for the following sites: Ha Makotoko, Ntloana Tsoana, Tloutle (Smith et al., 2002), and Sehonghong Rockshelter (Loftus et al., 2015), Lesotho; Boomplaas Cave (Sealy et al., 2016), Elands Bay Cave (Stowe & Sealy, 2016), Equus Cave (Lee-Thorp & Beaumont, 1995), Nelson Bay Cave (Sealy et al., 2020), Rose Cottage Cave (Smith et al., 2002), Sibhudu (Robinson & Wadley, 2018), and Wonderwerk Cave (Ecker et al., 2018), South Africa; and Kalemba Rockshelter (Robinson, 2017) and Makwe Rockshelter (Robinson & Rowan, 2017), Zambia. Even though Zambia is not typically considered part of southern Africa in MSA and LSA archaeology, these sites are included here as Val

& Collins (2022) explicitly argue that a broader regional comparison of environmental datasets is necessary. Furthermore, regional analysis of Kalahari dune fields (Thomas & Burrough, 2016) and southern African climate models (Chase, 2021) increasingly incorporates the Zambezi Basin. For most of the sites, except those in Lesotho and Rose Cottage Cave, isotope analysis was conducted on the entire late Pleistocene and Holocene archaeological sequence available at the time of study and included all potential herbivores represented by teeth viable for study. Sampling only targeted MSA layers of MIS 3 (~ 35,000–33,000 years ago (ya)) at Sehonghong (Loftus et al., 2015) and the post-LGM period, including Holocene layers, at Rose Cottage Cave (Smith et al., 2002). Isotopic analyses at Ha Makotoko and Ntloana Tsoana include few taxa, with just wildebeest (*Connochaetes* sp.) and zebra (*Equus* sp.) sampled at Ha Makotoko and only zebra samples from Ntloana Tsoana (Smith et al., 2002). Additionally, these samples, along with those from Tloutle, which includes a greater array of species, are quite small (Ha Makotoko, $n = 9$; Ntloana Tsoana, $n = 7$; Tloutle, $n = 12$; Smith et al., 2002). These sites are included here for completeness, but the results from these sites are very preliminary.

For this study, the sequences at each site are divided into seven temporal bins: ~ 70,000–50,000 ya, ~ 49,900–36,000 ya, ~ 35,900–25,000 ya, ~ 24,900–15,000 ya, ~ 14,900–11,000 ya, ~ 10,900–5000 ya, and ~ 4900–500 ya (Table 1). I use the "ya" terminology for chronology here as methods applied to the dating of the study sites include optically stimulated luminescence, uranium series, amino acid racemization, and Bayesian modeling approaches in addition to radiocarbon determinations (Supplemental Dataset 1 in Online Resource 1). These methods yield dates on different temporal scales for measuring chronology, and not all of them are directly comparable to the before present (BP) timescale commonly referenced for radiocarbon determinations. These temporal bins utilize Lombard and colleagues' (2022) recent update on the South African Stone Age sequence as a guideline but are also constructed to ensure meaningful isotopic sample sizes. As Lombard et al. (2022) do, I also recognize that there are some significant overlaps in the probable chronostratigraphic framework of southern African techno-complexes across sites, meaning that cultural sequences from each site do not neatly fall into specific temporal bins (see also Knight & Fitchett, 2021). The rough correlation of temporal bins and stages of the southern African sequence following Lombard et al. (2022) is as follows: Howiesons Poort (HP) and post-HP in the ~ 70,000–50,000-ya bin; here, I split the final MSA into the ~ 49,900–36,000-ya and ~ 35,900–25,000-ya bins as is warranted by a gap in radiometrically dated samples between ~ 38,000 and ~ 35,000 ya; the ~ 24,900–15,000-ya bin approximates the early LSA and Robberg parts of the sequence, although it is noted that the final MSA and early LSA overlap substantially on Lombard et al.'s (2022) timeline; ~ 14,900–11,000-ya, ~ 10,900–5000-ya, and ~ 4900–500-ya terminal Pleistocene-Holocene bins are constructed to maintain useful sample sizes and do not neatly match onto the techno-complexes. Keeping to the purpose of the sequence presented in Lombard et al. (2022), these bins are intended to be useful categories for investigating large datasets and broad trends, but do not suggest cultural assumptions. There are a number of different decisions in developing these temporal bins, and other researchers may justifiably find their way to different configurations. This is intended to simply be one potential option as the

Table 1 Division of the study sites into temporal bins

Temporal bin	Site (*n*)	Stratigraphic units
–	Sibhudu (29)	Pre-Still Bay
~70–50 ka	Sibhudu (69)	Still Bay, Howiesons Poort, post-Howiesons Poort
	Boomplaas Cave (26)	OCH, LOH, BOL
~49.9–36 ka	Sibhudu (18)	Late Middle Stone Age and final Middle Stone Age
	Boomplaas Cave (17)	OLP, BP
	Kalemba Rockshelter (2)	Horizon G
~35.9–25 ka	Boomplaas Cave (17)	YOL, LPC
	Equus Cave (16)	2b
	Sehonghong Rockshelter (29)	All units (I, J, K)
	Kalemba Rockshelter (61)	Horizons H, I, J, K (bottom)
~24.9–15 ka	Boomplaas Cave (26)	LP, GWA/HCA
	Elands Bay Cave (1)	SOSE
	Equus Cave (10)	2a
	Nelson Bay Cave (80)	YSL/YSG, YSL, YSG, GYGL
	Rose Cottage Cave (10)	DB-UP, DB-LR
	Kalemba Rockshelter (19)	Horizons K (top), L, M, N
~14.9–11 ka	Boomplaas Cave (49)	CL, BRL, BLA
	Elands Bay Cave (30)	SMOK, PBGB, GBSI, GBAN, FRTU, FOAM, BENE, ASHE
	Equus Cave (13)	1b
	Nelson Bay Cave (69)	GSL, GBSL/Shelly, GBSL, CS, BSL, BSJ
	Wonderwerk Cave (12)	4d/undefined
	Ha Makotoko (3)	BLOS-UR, BLOS-LR
	Ntloana Tsoana (4)	L/M14, BLOS
	Tloutle (2)	BC

Table 1 (continued)

Temporal bin	Site (*n*)	Stratigraphic units
~10.9–5 ka	Elands Bay Cave (34)	SLOPE, SHAK, PELE, PAR1, NEPT, LIRO, GONE, GNOM, ELFO, DECE, BSP2, BSP1, BSBP, BSBJ, BSAN
	Nelson Bay Cave (45)	Rice C + D, Rice C, Rice B, Rice A, Jake, Ivan, C (Rice C)
	Rose Cottage Cave (35)	Pt-UP, Pt-LR, Ph, JaG, Ja, HaPit, Ha, DCM, Cm
	Wonderwerk Cave (183)	4a, 4aLH, 4b, 4c/Auburn Sand, Dark Lens, Another Auburn Sand, Compacted Beige Sand
	Ha Makotoko (6)	GWA, BLOS-UR, BLOS-LR
	Ntloana Tsoana (3)	MCS, L/M14
	Tloutle (10)	CSL-UP, CSL, LR, BS
	Kalemba Rockshelter (11)	Horizons O, P, Q
	Makwe Rockshelter (47)	Horizons 1, 2i, 2ii, 3i, 3ii
~4.9 ka–500 ya	Boomplaas Cave (1)	DGL
	Elands Bay Cave (20)	LIAP, JOFR, GEOB, GASO, DOLL, DOLA, CCLA BADI
	Equus Cave (4)	1a
	Nelson Bay Cave (19)	Vincent, Reg, Geoff, Edward, Dan, Clara, Cedric, BSBI, BSBG/H, BSB
	Rose Cottage Cave (19)	Mn, A2, A
	Wonderwerk Cave (126)	2b, 3a, 3b/Fine Brown Sand, Brown with White speckles
	Makwe Rockshelter (62)	Horizons 4i, 4ii, 5

first attempt to compile the entire existing southern African faunal enamel isotope record to address an "on the ground" expression of regional environmental trends.

Materials and Methods

Samples and Temporal Bin Construction

All previously published ($n = 1235$) faunal enamel isotope samples, including grazers and browsers, were compiled (Supplemental Dataset 1 in Online Resource 1) for the 13 study sites: Ha Makotoko, Ntloana Tsoana, Tloutle, and Sehonghong (Lesotho); Boomplaas Cave, Elands Bay Cave, Equus Cave, Nelson Bay Cave, Rose Cottage Cave, Sibhudu, and Wonderwerk Cave (South Africa); and Kalemba and Makwe rockshelters (Zambia) (Fig. 1; Table 1). Taxonomic information for each specimen is provided by the original isotope studies. This dataset is supplemented by 12 additional, previously unpublished, samples as follows: four cercopithecoid primate samples from Sibhudu; three samples of *Papio* sp. (baboon), one *Hystrix* sp. (porcupine), and one sample of *Sylvicapra grimmia* (common forest duiker) from Kalemba Rockshelter; and two samples of *Hystrix* sp. and one cercopithecoid primate from Makwe Rockshelter (see Supplemental Dataset 1) following standard processing and characterization protocols (see Supplementary Methods in Online Resource 2 for details). Despite the development of a number of stable isotope datasets from late Pleistocene and Holocene southern Africa sites, there are no published values for non-human primates. In addition to being incorporated into the broader multi-site analyses of southern Africa, a detailed assessment of the primate samples is also conducted and provided in the Supplementary Results (Online Resource 2: Table S1; Fig. S1).

Chronological data and published ages were collected for all sites and for each stratigraphic unit, if available, for which stable isotope samples came from in order to construct temporal bins. These datasets are primarily radiocarbon (both conventional and AMS) dates on material like ostrich eggshell (OES) carbonates and charcoal, but also optically stimulated luminescence (OSL) dates in the case of Sibhudu (Jacobs et al., 2008a, 2008b), and Bayesian statistical models that incorporated both old and new radiocarbon dates for Boomplaas Cave (Pargeter et al., 2018), Nelson Bay Cave (Loftus et al., 2016), and Rose Cottage Cave (Loftus et al., 2019). All radiocarbon dates were calibrated with OxCal 4.4 (Bronk Ramsey, 2009) with the updated SHCal20 Southern Hemisphere calibration curve (Hogg et al., 2020) and reported at 2σ. Due to the new SHCal20 calibration curve, all sites with radiocarbon dates were calibrated, even those for which calibrated radiocarbon dates have previously been published. As a result, some of the calibrated dates in Supplemental Dataset 1 (Online Resource 1) may be slightly different from previously published calibrated dates. Where multiple radiocarbon determinations were available for a specific stratigraphic layer, an average was constructed. OSL dates from Sibhudu do not require calibration. Bayesian model dates were only used for stratigraphic layers from which no physical date was available. Determining the age of layers for which no dates and no model were available relied on estimations provided in publications

or interpretations based on the age of stratigraphic layers above and below. Original or modeled dates, as well as the calibrated "age used" dates, are available for all samples in Supplemental Dataset 1.

Isotope Space Analyses

$\delta^{13}C_{enamel}$ and $\delta^{18}O_{enamel}$ analyses of the tooth enamel of African fauna, including primates, are a well-established method of paleodietary and paleoenvironmental reconstruction (e.g., Cerling et al., 2003, 2015; Levin et al., 2015; Sponheimer et al., 2003) whereby $\delta^{13}C_{enamel}$ signatures are related to the isotopic composition of vegetation consumed (Ambrose & DeNiro, 1986; Cerling et al., 2003; Sponheimer et al., 2003) and $\delta^{18}O_{enamel}$ values are often utilized as a proxy of local hydrological conditions (Blumenthal et al., 2017; Levin et al., 2009). Measuring isotope space offers the potential to capture ecological niches, defined as a multi-dimensional space with axes representing resources (bionomic), here represented by $\delta^{13}C_{enamel}$ values, and bioclimatic factors (scenopoetic), represented by $\delta^{18}O_{enamel}$ values, in comparing study sites (Eckrich et al., 2020; Hutchinson, 1957). As the chemical composition of tooth enamel is a reflection of what an animal consumes and its habitat, calculating isotope space and overlap based on these isotope systems ($\delta^{13}C_{enamel}$ and $\delta^{18}O_{enamel}$) allows for a way to quantitatively compare the niches of different groups. To avoid confusion of the terms isotope niche and trophic niche (of which isotope niche only captures a part of), I prefer to utilize the terms isotope space and isotope space overlap for these analyses (see Hette-Tronquart, 2019, for a detailed discussion).

Modern C_3 plants (primarily trees, shrubs, and high-altitude grasses) in Africa have a $\delta^{13}C$ range of -36 to $-22‰$ with a mean of $-26.4 \pm 2.1‰$ while C_4 plants (low-elevation tropical grasses, sedges, and shrubs of the Amaranthaceae) in Africa have a $\delta^{13}C$ range of -14 to $-11‰$ and a mean of $-11.4 \pm 1.3‰$, when corrected to the pre-industrial value of the atmosphere for purposes of comparing to the archaeological record (Cerling, 2014). Variation in $\delta^{13}C$ values of C_3 plants is due to environmental factors like temperature and moisture availability where cooler, wetter conditions result in more negative values (Diefendorf et al., 2010; Kohn, 2010). In southern Africa, this pattern is complicated by the existence of the WRZ and YRZ and the high-elevation environments of Lesotho. WRZ fynbos vegetation, including grasses and sedges, primarily utilizes the C_3 pathway (Vogel, 1978) whereas SRZ grasses are predominantly C_4 plants (Mucina & Rutherford, 2006). In Lesotho, there is an altitudinal gradient with temperature and precipitation that results in C_3 grasses being found at higher elevations that differ on north-facing (~2700 m) and south-facing (~2100 m) slopes (Cowling, 1983; Parker et al., 2011; Vogel, 1978). Following Sealy et al. (2020), the $\delta^{13}C_{enamel}$ values of all samples were corrected for changes in atmospheric pCO_2; however, since these corrections did not lead to changes in the overall results, they are only discussed in the Supplementary Results (Online Resource 2) with the isotope space measures using the originally published, unaltered, values. It is recognized here that interpreting diets and, in turn, paleoecological conditions, from $\delta^{13}C_{enamel}$ values, can lead to oversimplifications, especially

in southern Africa where similar diets, like feeding on grasses that utilize the C_3 versus C_4 pathway, could lead to different isotopic signatures, and different diets, such as feeding on C_3 grasses versus C_3 woody vegetation, would lead to similar signatures. That said, the importance and presence of C_3 grasses in southern Africa can be turned into an analytical strength. Isotope space measures have the potential to identify clear differences among study sites and within sites through time, when applied to those taxa which are expected to be grazing fauna based on previous zooarchaeological studies as described below.

$\delta^{18}O_{enamel}$ values provide environmental and/or climatic information based on the sources of precipitation, oxygen isotope composition of drinking water, water derived from food, and inspired oxygen. $\delta^{18}O_{enamel}$ values are thought to reflect aridity (Blumenthal et al., 2017; Levin et al., 2006) and, perhaps, seasonality of precipitation (Sealy et al., 2020). In the southern African context, a modern study of precipitation in Cape Town found winter rain to be depleted in ^{18}O (Harris et al., 2010); however, this has not been directly replicated in archaeological studies (Stowe & Sealy, 2016). C_3 plants tend to have enriched values compared to C_4 vegetation due to differences in the rate of evapotranspiration, resulting in browsing taxa that receive most of their water from ingested leaf water having higher $\delta^{18}O_{enamel}$ values and tracking evaporative water deficit compared with grazing taxa that rely on surface water sources (Cerling et al., 2008). Differences in how plants of the two photosynthetic pathways incorporate $\delta^{18}O$ values into their tissues may be one factor in complicating the patterns when compared to measures of winter and summer rainfall directly. $\delta^{18}O_{enamel}$ values may provide insight to past climatic and hydrological conditions but must be interpreted cautiously as the relationship between $\delta^{18}O_{enamel}$ and meteoric water, diet, and atmospheric oxygen is incompletely understood (Faith, 2018; Levin et al., 2009). With such a large geographic area and many diverse environments sampled among the study sites, it is likely that different sources of precipitation are represented. As such, direct comparison of specific $\delta^{18}O_{enamel}$ values may not be justified, but general trends in $\delta^{18}O_{enamel}$ values in combination with $\delta^{13}C_{enamel}$ values in isotope space have been interpreted to reveal potentially important environmental and ecological conditions (Robinson, 2022; Lüdecke et al., 2022).

Statistical Analyses

Isotope space measures are calculated for grazing taxa with the rKIN package (Eckrich et al., 2020) in R which provides the possibility of analyzing datasets using three models: minimum convex polygons (MCPs), standard ellipse area (SEA), and kernel utilization density (KUD). Isotope space is defined as the total spatial area encompassing data points with the different models handling sample size and uncertainties differently. As MCPs have been found to consistently underestimate isotope space size and overlap (Eckrich et al., 2020; Robinson, 2022), they are not calculated in this study. In SEA models, an ellipse is constructed around a pre-determined percentage of test data (referred to as a contour level or interval which is discussed further below) from which ellipse radii are calculated. This approach can reduce

sensitivity to sample size differences among study groups and outliers, but the model will always be in the shape of an ellipse that may include unused or exclude used areas of isotope space. Furthermore, elliptical models assume that isotope data are independent and normally distributed in multivariate space (Jackson et al., 2011), but many archaeological isotope studies are known or suspected to be prone to non-normality (Roberts et al., 2018). KUD models are generated by summing two separate kernel functions over observed data points with the total area defined as the minimum size that includes all data points under consideration free of distributional assumptions or pre-set grid shapes, such as ellipses (Eckrich et al., 2020). Interpreting total isotope space and assessing larger or smaller isotope space areas among groups within a study is contingent on the particularities of the question at hand, although smaller niche spaces typically indicate a less diverse resource base and/or specialized feeding and a restricted range of habitats (Eckrich et al., 2020; Newsome et al., 2007; Robinson, 2022).

Isotope space overlap is calculated as the size of the overlapping region between the isotope space area size of group A and the isotope space area size of group B divided by the total isotope space area size of group B. This measure can also be calculated in reverse to get a measure of how much group B overlaps group A (Eckrich et al., 2020). In the current study, the greater the percentage of overlap, the higher the inferred dietary and/or environmental overlap would be depending on if the overlap primarily occurs along the axis upon which $\delta^{13}C_{enamel}$ or $\delta^{18}O_{enamel}$ is plotted. Little or no overlap of isotope space between two groups would indicate different dietary or environmental circumstances. Again, specifics of the research question and the nature of the study groups would determine what percentages of overlap are consequential. Here, I consider overlap at $>60\%$ to be high, likely indicating quite similar dietary and/or environmental conditions. For more details on how isotope space and overlap is calculated and the application of these methods to archaeological studies, see Robinson (2022).

Each enamel sample was classified as either a browser, mixed feeder, or grazer based on taxonomic identification and feeding/habitat preference of modern analogs (e.g., Kingdon, 1982, 2015) with a focus on dietary analyses conducted on southern African fauna (e.g., Codron et al., 2007, 2008; Gagnon & Chew, 2000; Skinner & Chimimba, 2005). Dietary classifications mostly follow those in Sealy et al. (2020), although there are a few differences. Here, *Oreotragus oreotragus* (klipspringer) is classified as a browser (Skinner & Chimimba, 2005), although Sealy et al. (2020) cite evidence of grazing on fresh grass in Ethiopia to place klipspringer in a mixed feeding category. Similarly, Sealy et al. (2020) categorize *Ourebia ourebi* (oribi) as a grazer based on seasonal dietary variability (Gagnon & Chew, 2000), but this species is placed with the mixed feeders here following Cerling et al., (2003, 2015). There is also additional fauna not present in Sealy et al. (2020). Despite low $\delta^{13}C_{enamel}$ values, following Brink's (1999) analysis of dental anatomy, Sealy et al. (2016) consider the unnamed caprine from Boomplaas to be a C_3 grazer and it is classified as a grazer here. A small number of samples identified as *Tragelaphus strepsiceros* (greater kudu; Clark, 2017) from the post-HP at Sibhudu ($n=4$) have a $\delta^{13}C_{enamel}$ range of -1.1 to $1.6‰$ which is much higher than any known modern or fossil kudu values. As a result, I treat these samples as *Tragelaphus* sp. and place

Table 2 Common and scientific names for dietary category groupings

Dietary category	Scientific name	Common name
Grazers	*Aepyceros melampus*	Impala
	Alcelaphus buselaphus	Hartebeest
	Antidorcas bondi	Bond's springbok
	–	Boomplaas caprine
	Ceratotherium simum	White rhinoceros
	Connochaetes gnou	Black wildebeest
	Connochaetes taurinus	Blue wildebeest
	*Damaliscus dorcas**	Blesbok
	*Damaliscus pygargus**	Blesbok
	Hippotragus equinus	Roan antelope
	Hippotragus leucophaeus	Bluebuck
	Hippotragus niger	Sable antelope
	Kobus ellipsiprymnus	Waterbuck
	Megalotragus priscus	–
	Redunca arundinum	Southern reedbuck
	Redunca fulvorufula	Mountain reedbuck
	Syncerus caffer	African buffalo
	Syncerus antiquus	Giant African buffalo
	Tragelaphus sp.	Sibhudu tragelaphin
	Equus capensis	Cape zebra
	Equus quagga	Plains zebra
	Equus zebra	Mountain zebra
	Hippopotamus amphibius	Hippopotamus
	Phacochoerus sp.	Warthog
	Pedetes capensis	South African springhare

them in the grazer category. Domesticated *Bos taurus* and *Caprini* sp. from Makwe are separated out from the grazers. Primates, while perhaps more appropriately classified as omnivores, are placed in the browser category here due to their low $\delta^{13}C_{enamel}$ values (Table 2; Online Resource 1).

In addition to the models, isotope space measures are generated at three common contour intervals: 50%, 75%, and 95%. Contour intervals provide the ability to measure isotope space size as the area encompassed by the contours of a particular percent of data in the dataset. Lower contour values prevent outliers or other extreme data points from significantly influencing estimates of isotope space size or overlap. Best practices call for calculating isotope space size at multiple contour intervals to assess the stability of model measurements and to identify how outliers may be affecting isotope space measures (Eckrich et al., 2020; Robinson, 2022). Eckrich et al. (2020) determined that a minimum of 10 samples was required to calculate reliable and realistic estimates of isotope space and overlap using rKIN. A *smallSamp*() function allowing analyses to be run with as few as five samples is built into rKIN and is used here to calculate isotope space measures for analytical units

Table 2 (continued)

Dietary category	Scientific name	Common name
Mixed Feeders	*Eudorcas thomsonii*	Thomson's gazelle
	Ourebia ourebi	Oribi
	Procavia capensis	Rock hyrax
Browsers	*Antidorcas marsupialis*	Springbok
	Cephalophus natalensis	Red forest duiker
	Oreotragus oreotragus	Klipspringer
	Pelea capreolus	Grey rhebok
	Philantomba monticola	Blue duiker
	Raphicerus campestris	Steenbok
	Raphicerus melanotis	Cape grysbok
	Sylvicapra grimmia	Common duiker
	Tragelaphus oryx	Eland
	Tragelaphus scriptus	Bushbuck
	Tragelaphus strepsiceros	Greater kudu
	Potamochoerus sp.	Bushpig
	Cercopithecus albogularis	Sykes' monkey
	Chlorocebus pygerythrus	Vervet monkey
	Papio sp.	Baboon
	Hystrix sp.	Porcupine
Domesticates	*Bos taurus*	Cattle
	Caprini sp.	Sheep/goat

Damaliscus dorcas is now known as *Damaliscus pygargus*, but the original identifications of *Damaliscus dorcas* from Smith et al. (2002) are preserved in this study

represented by nine samples to increase the number of sites that can be included. rKIN models are applied to the grazer portion of the study site assemblages as a whole and within each temporal bin. Due to the small sample sizes, the Lesotho sites of Ha Makotoko and Ntloana Tsoana are not analyzed with isotope space models. Tloutle is represented by 10 grazers in the ~ 10,900–5000-ya bin and is included only in this temporal section. Sehonghong, with isotope samples dating only to the ~ 35,900–25,000-ya bin, and Sibhudu, with all samples dating to earlier than ~ 38,000 ya, are excluded from the full site comparison to avoid an overly complicated visualization of isotope space and overlap. Equus Cave is excluded from the isotope space measures as there are no $\delta^{18}O_{enamel}$ values directly associated with the published $\delta^{13}C_{enamel}$ values from the site.

In addition to the isotope space measures, descriptive statistics and a series of traditional non-parametric statistical analyses comparing the sites and temporal bins are conducted (Online Resource 2: Tables S2–S26). Further comparisons took the form of ternary diagrams and probability density functions (PDFs). These analyses are meant to supplement the primary rKIN modeling, and I provide a description of them in the Supplementary Methods (Online Resource 2: Supplementary Results; Figs. S1 and S2). In particular, these approaches allow for some analyses

not possible with the isotope space measures as follows: (1) a comparison of the $\delta^{13}C_{enamel}$ values from Equus Cave with $\delta^{13}C_{enamel}$ values from the other study sites, (2) analysis and comparison of the browsing dietary category among the study sites, and (3) consideration of species-level comparisons for the most commonly sampled taxa across the study sites. Specific results of these analyses that contribute to the overall regional paleoenvironmental reconstruction are described in the main text, but a full analysis of these results is provided in the Supplementary Results (Online Resource 2).

All of these sites have been subject to intensive site-specific analyses. It is not the purpose of the present study to re-analyze the site level results or interpretations, but instead to apply a hierarchical approach to reconstructing environmental conditions across southern Africa as an integrated landscape based on local datasets. To this end, the following hypotheses have been developed which can be tested directly with the isotope space approach:

- Sites in the five broadly defined environmental zones—the WRZ, the YRZ, the SRZ, the Lesotho highlands, and interior southern Africa including the Zambezi region—will occupy different areas of isotope space, and those in the same zone will have high levels of isotope space overlap.
- Sites experiencing winter rainfall will occupy narrower areas of isotope space, and changes in rainfall seasonality over time can be identified by expansions or contractions of isotope space. Modern winter rainfall in the Western Cape has been found to be depleted in ^{18}O, resulting in lower overall $\delta^{18}O$, compared with rain that falls during summer months (Diamond & Harris, 2019; Harris et al., 2010). On a regional scale, $\delta^{18}O$ values of precipitation modeled from groundwater largely replicate this pattern with depleted $\delta^{18}O$ values along the Atlantic Coast, the most enriched $\delta^{18}O$ values in the eastern Cape, and highly variable $\delta^{18}O$ values in the interior which receives rain in both the summer and winter months (West et al., 2014). Therefore, it is expected that sites experiencing predominantly winter rainfall and those receiving primarily summer rainfall will not overlap in isotope space. When (and if) sites in the WRZ start to receive more summer rain, their isotope space should increase and begin to overlap more with sites in the YRZ and, perhaps, the SRZ. In turn, when (and if) the WRZ expands into the present-day YRZ, the isotope space of sites within the YRZ should contract in size.

Results

Site Comparisons

Both the SEA and KUD models offer similar results with only minor differences that have no bearing on the overall interpretations here. Results based on the analysis of the KUD model are reported in the main text as this model appears to capture isotope space measures more accurately; however, constructed ellipses and results of the SEA model are also reported in the figures and tables in the interest of full

transparency. The seven study sites which are analyzed using all grazer samples irrespective of temporal bin appear to fall into two groups in terms of the amount of isotope space occupied (Fig. 2; Table S27). Elands Bay Cave, Nelson Bay Cave, and Wonderwerk Cave are estimated to occupy a slightly smaller isotope space than Boomplaas Cave, Rose Cottage Cave, Kalemba Rockshelter, and Makwe Rockshelter. Elands Bay Cave isotope space is overlapped meaningfully by only Boomplaas Cave (~30–40%) at the 50% and 75% contour levels and overlapped by up to a maximum of ~20% by the other sites at exclusively the 95% contour level (Table 3). Boomplaas Cave isotope space is overlapped by Elands Bay Cave and Rose Cottage Cave to a moderate degree at the 50% and 75% contours. Rose Cottage Cave and Wonderwerk Cave overlap > 30% at all contour levels, but Wonderwerk Cave isotope space is not overlapped by Boomplaas Cave. Isotope spaces of Nelson Bay Cave and the Zambian sites of Kalemba and Makwe rockshelters overlap each other at each of the contour intervals, but the Zambian sites are characterized by expansion along the $\delta^{13}C_{enamel}$ axis indicating C_4-dominated environments (Fig. 2; Table 3).

Temporal Changes

The Kruskal–Wallis tests find that $\delta^{13}C_{enamel}$ and $\delta^{18}O_{enamel}$ values of many of the test sites have statistically significant changes across temporal bins (Online Resource 2: Supplementary Results; Fig. S4; Tables S28–S30). This suggests that there may be changes to the amount of isotope space occupied and the patterns of overlap through time.

Approximately 70,000–50,000 ya

Only Boomplaas Cave and Sibhudu yield sufficient isotope samples dating to the earliest temporal bins. In the ~70,000–50,000-ya bin, Boomplaas Cave is found to occupy a smaller isotope area than Sibhudu (Fig. S5; Tables S31 and S32). Of grazer samples, 25% from Boomplaas have $\delta^{13}C_{enamel}$ values $< -8.0‰$ with the remainder in the mixed-feeding range of $-8.0‰ \leq \delta^{13}C_{enamel}$ values $\leq -1.0‰$, while Sibhudu grazers are found to have diets dominated by C_4 vegetation with > 50% as C_4 feeders. Estimated consumption of C_3 resources by grazers at Boomplaas Cave is ~40–50%, but only ~15–25% at Sibhudu.

Approximately 49,900–36,000 ya

Both sites occupy less isotope space in the ~49,900–36,000-ya period than in the ~70,000–50,000-ya bin. Overlap is estimated at < 10% (Fig. S6; Tables S33 and S34). These patterns reflect Sibhudu having significantly lower grazer $\delta^{18}O_{enamel}$ values and higher grazer $\delta^{13}C_{enamel}$ values than Boomplaas. At both sites, C_4 consumption is estimated to be similar to the preceding temporal bin (Fig. S7; Tables S6–S11). Over 90% of Boomplaas grazers are categorized as C_3 dominated or mixed feeding in the ~49,900–36,000-ya period while > 80% of Sibhudu grazers are classified as predominantly C_4 feeding (Fig. S3).

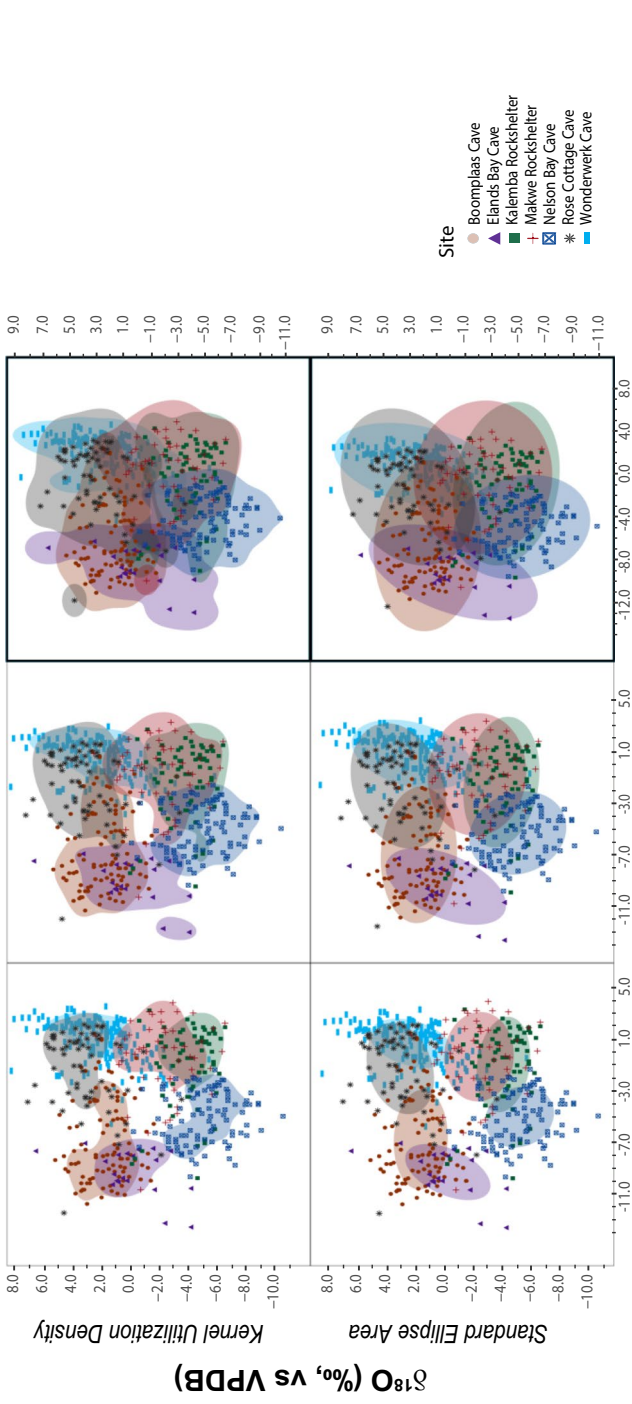

Fig. 2 Niche size and overlap for all grazer samples from individual study sites regardless of temporal bin. Rows represent different estimation methods (standard ellipse area (SEA) and kernel utilization density (KUD)). Columns display results at commonly selected contour levels of 50%, 75%, and 95%. In order to ensure that all plots present with equal proportions, the scales for the SEA and KUD methods at 95% differ. This is indicated by the thicker weight of the box boarder for these plots. VPDB, Vienna Pee Dee Belemnite

Table 3 Pair-wise isotopic niche overlaps from standard ellipse area (SEA) and kernel utilization density (KUD) for all grazers regardless of temporal bin

Method	Group	Boomplaas Cave			Elands Bay Cave			Nelson Bay Cave			Rose Cottage			Wonderwerk			Kalemba RS			Makwe RS		
		50%	*75%*	*95%*	*50%*	*75%*	*95%*	*50%*	*75%*	*95%*	*50%*	*75%*	*95%*	*50%*	*75%*	*95%*	*50%*	*75%*	*95%*	*50%*	*75%*	*95%*
SEA	**BC**	–	–	–	*0.30*	*0.41*	*0.50*	0.00	0.00	*0.10*	*0.12*	*0.35*	*0.56*	0.00	*0.01*	*0.20*	0.00	0.00	*0.11*	0.00	*0.05*	*0.30*
	EBC	*0.39*	*0.54*	*0.64*	–	–	–	0.00	0.00	*0.16*	0.00	0.00	*0.10*	0.00	0.00	0.00	0.00	0.00	*0.07*	0.00	0.00	*0.08*
	NBC	0.00	0.00	*0.13*	0.00	0.00	*0.17*	–	–	–	0.00	0.00	*0.06*	0.00	0.00	*0.03*	*0.15*	*0.38*	*0.60*	0.00	*0.20*	*0.49*
	RCC	*0.11*	*0.31*	*0.50*	0.00	0.00	*0.18*	0.00	0.00	*0.04*	–	–	–	*0.34*	*0.48*	*0.57*	0.00	0.00	*0.08*	0.00	*0.08*	*0.33*
	WC	0.00	*0.02*	*0.25*	0.00	0.00	0.00	0.00	0.00	*0.03*	*0.47*	*0.66*	*0.80*	–	–	–	0.00	0.00	*0.20*	*0.03*	*0.26*	*0.48*
	KR	0.00	0.00	*0.11*	0.00	0.00	*0.06*	*0.12*	*0.32*	*0.49*	0.00	0.00	*0.10*	0.00	0.00	*0.17*	–	–	–	*0.54*	*0.70*	*0.83*
	MR	0.00	*0.04*	*0.26*	0.00	0.00	*0.05*	0.00	*0.32*	*0.33*	0.00	*0.08*	*0.32*	*0.02*	*0.18*	*0.33*	*0.44*	*0.57*	*0.67*	–	–	–
KUD	**BC**	–	–	–	*0.39*	*0.43*	*0.46*	0.00	0.00	*0.10*	*0.02*	*0.29*	*0.62*	0.00	*0.03*	*0.25*	0.00	0.00	*0.12*	0.00	*0.02*	*0.35*
	EBC	*0.61*	*0.54*	*0.52*	–	–	–	0.00	*0.09*	*0.19*	0.00	*0.01*	*0.24*	0.00	0.00	0.00	0.00	0.00	*0.18*	0.00	0.00	*0.16*
	NBC	0.00	0.00	*0.13*	0.00	0.00	*0.22*	–	–	–	0.00	0.00	*0.18*	0.00	0.00	*0.08*	*0.05*	*0.33*	*0.59*	0.00	*0.24*	*0.49*
	RCC	*0.03*	*0.30*	*0.50*	0.00	*0.01*	*0.17*	0.00	0.00	*0.11*	–	–	–	*0.37*	*0.41*	*0.50*	0.00	0.00	*0.14*	0.00	*0.07*	*0.35*
	WC	0.00	*0.05*	*0.30*	0.00	0.00	0.00	0.00	0.00	*0.08*	*0.55*	*0.62*	*0.75*	–	–	–	0.00	*0.04*	*0.24*	*0.13*	*0.36*	*0.50*
	KR	0.00	0.00	*0.13*	0.00	0.00	*0.17*	*0.05*	*0.31*	*0.49*	0.00	0.00	*0.18*	0.00	*0.03*	*0.21*	–	–	–	*0.57*	*0.77*	*0.80*
	MR	0.00	*0.02*	*0.30*	0.00	0.00	*0.12*	0.00	*0.17*	*0.33*	0.00	*0.06*	*0.37*	*0.07*	*0.21*	*0.36*	*0.39*	*0.58*	*0.65*	–	–	–

Overlaps provided at 50%, 75%, and 95% contour intervals. Italicized values indicate where overlap is estimated

Approximately 35,900–25,000 ya

Boomplaas Cave and Sehonghong occupy less isotope space than Kalemba Rockshelter in this period (Table S35). Overlaps are estimated at > 30% at all contour levels for Boomplaas Cave and Sehonghong. Estimates of overlap with Kalemba Rockshelter are < 11% and are only found at the 95% contour (Fig. 3; Table 4). Compared with the earlier temporal bins, Boomplaas is calculated to occupy approximately the same isotope space as in the ~ 49,900–36,000-ya interval. While not included in the rKIN analyses, Equus Cave grazer $\delta^{13}C_{enamel}$ values are found to be significantly higher than those at Boomplaas Cave or Sehonghong, but lower than grazer $\delta^{13}C_{enamel}$ values at Kalemba Rockshelter (Fig. S8; Tables S12–S14). Grazers from Boomplaas Cave and Sehonghong are estimated to have consumed ~ 65–75% of C_3 resources, with > 50% of grazer samples from each of these sites with isotopically determined C_3-dominated diets. Grazers from Equus Cave and Kalemba Rockshelter are found to have consumed only ~ 15–25% of C_3 plants with > 40% of grazers from both sites indicating traditional C_4-dominated diets (Fig. S3). $\delta^{18}O_{enamel}$ values of the three sites for which they are available are all significantly different from each other, with Kalemba Rockshelter (-4.3 ± 1.6‰; $n = 61$) having the lowest values and Boomplaas Cave (1.7 ± 2.4‰; $n = 17$) the highest (Fig. S8; Table S12).

Approximately 24,900–15,000 ya

Rose Cottage Cave is estimated to occupy the most isotope space in this temporal bin and Kalemba Rockshelter the least. Kalemba Rockshelter is found to occupy only approximately two-thirds of the isotope space in this interval compared with ~ 35,900–25,000-ya bin. Boomplaas isotope space approximately doubles in this bin compared with the ~ 35,900–25,000-ya one (Fig. 4; Table S36). Kalemba Rockshelter isotope space is overlapped by that of Nelson Bay Cave and Rose Cottage Cave on the order of ~ 10–20% at the 95% contour interval. Boomplaas Cave and Rose Cottage Cave isotope space overlaps at ~ 35–50% at the 95% interval (Table 5).

Rose Cottage Cave (-3.1 ± 2.6‰; $n = 10$) and Kalemba Rockshelter (-0.7 ± 2.9‰; $n = 13$) are found to have similar grazer $\delta^{13}C_{enamel}$ values to Equus Cave (-1.7 ± 2.0‰; $n = 6$). All other pairs comparing grazer $\delta^{13}C_{enamel}$ values are found to have statistically significant differences. Boomplaas Cave has the lowest grazer $\delta^{13}C_{enamel}$ values and Kalemba Rockshelter the highest (Fig. S9; Tables S15–S17). Grazers at Boomplaas Cave and Nelson Bay Cave are estimated to have consumed > 50% of C_3 resources, while those at the other three sites < 30%. Most grazers (> 60%) from Equus Cave, Nelson Bay Cave, and Rose Cottage Cave are found to have mixed-feeding $\delta^{13}C_{enamel}$ values. More than 60% of grazers from Boomplaas Cave have $\delta^{13}C_{enamel}$ values < -8.0‰. Only Kalemba Rockshelter (~ 70%) has a majority of grazer samples with C_4-dominated diets (Fig. S3). Boomplaas Cave has the highest $\delta^{18}O_{enamel}$ values (2.0 ± 1.6‰; $n = 25$), similar to those from Rose Cottage Cave (0.8 ± 2.3‰; $n = 10$). Nelson Bay Cave (-4.6 ± 2.2‰; $n = 51$) and Kalemba Rockshelter

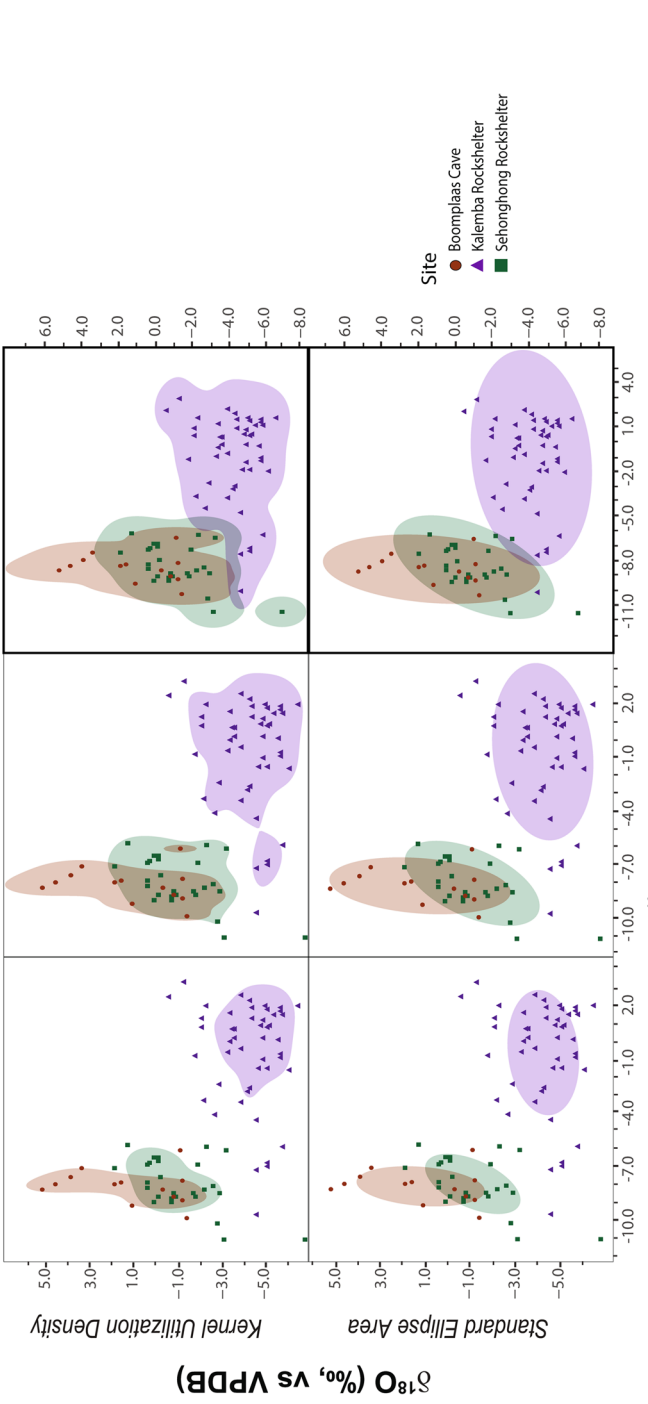

Fig. 3 Niche size and overlap for all grazer samples from individual study sites in the ~ 35,900–25,000-ya temporal bin. Rows represent different estimation methods (standard ellipse area (SEA) and kernel utilization density (KUD)). Columns display results at commonly selected contour levels of 50%, 75%, and 95%. In order to ensure that all plots present with equal proportions, the scales for the SEA and KUD methods at 95% differ. This is indicated by the thicker weight of the box boarder for these plots. VPDB, Vienna Pee Dee Belemnite

Table 4 Pair-wise isotopic niche overlaps from standard ellipse area (SEA) and kernel utilization density (KUD) for all grazers in the ~ 35,900–25,000-ya temporal bin

Method	Group	Boomplaas Cave			Sehonghong			Kalemba Rockshelter		
		50%	*75%*	*95%*	*50%*	*75%*	*95%*	*50%*	*75%*	*95%*
SEA	**BC**	–	–	–	*0.33*	*0.49*	*0.61*	0.00	0.00	*0.01*
	SH	*0.34*	*0.50*	*0.63*	–	–	–	0.00	0.00	*0.04*
	KR	0.00	0.00	0.00	0.00	0.00	*0.02*	–	–	–
KUD	**BC**	–	–	–	*0.45*	*0.56*	*0.70*	0.00	0.00	*0.01*
	SH	*0.45*	*0.53*	*0.60*	–	–	–	0.00	0.00	*0.11*
	KR	0.00	0.00	*0.01*	0.00	0.00	*0.08*	–	–	–

Overlaps provided at 50%, 75%, and 95% contour intervals. Italicized values indicate where overlap is estimated

(-3.7 ± 1.9‰; $n = 13$) have the lowest $\delta^{18}O_{enamel}$ values, both statistically lower than those from Boomplaas or Rose Cottage (Fig. S9; Tables S15–S17).

Approximately 14,900–11,000 ya

Only three of the seven sites with grazer specimens dated to this bin have large enough sample sizes for isotope space measures. Boomplaas Cave is found to occupy the largest amount of isotope space among the three, double the space occupied by this site in the ~ 49,900–36,000-ya and ~ 35,900–25,000-ya periods and slightly more than that in the ~ 24,900–15,000-ya bin. Elands Bay Cave and Nelson Bay Cave occupy approximately the same amount of isotope space, but do not overlap in isotope space at all (Fig. 5; Table S37). Boomplaas Cave isotope space overlaps the isotope space of Elands Bay Cave at ~ 40–45% at all contours, whereas with the opposite pattern, Elands Bay Cave overlaps Boomplaas Cave isotope space only at ~ 5–25%. Boomplaas Cave and Nelson Bay Cave are only found to have overlapped at the 95% contour level and only at ~ 1–2% (Table 6).

Wonderwerk Cave (0.0 ± 1.9‰; $n = 4$) and Equus Cave (-2.2 ± 1.8‰; $n = 10$) have the highest grazer $\delta^{13}C_{enamel}$ values in this temporal bin, both significantly higher than the values from any other site. Elands Bay Cave (-10.5 ± 1.7‰; $n = 10$) has the lowest grazer $\delta^{13}C_{enamel}$ values, significantly lower than those from any other site (Fig. S10; Tables S18–S20). Grazers from Elands Bay Cave are estimated to have consumed ~ 80–90% of C_3 plants, with those from Boomplaas Cave also estimated at > 50%. Estimated C_3 resource consumption for grazers at Equus Cave and Wonderwerk Cave is ~ 10–25%. Nelson Bay Cave falls in the middle with estimated grazer C_3 consumption of ~ 40% (Table S18). Only Wonderwerk Cave in this time period has a majority of grazer specimens with C_4-dominated diets. All other sites, except Elands Bay Cave, have > 40% of grazer samples with mixed-feeding diets. More than 90% of grazers from Elands Bay Cave are in the < -8.0‰ category (Fig. S3). Analysis of $\delta^{18}O_{enamel}$ values finds similar values for Boomplaas Cave and Wonderwerk Cave. Grazer $\delta^{18}O_{enamel}$ values (-5.7 ± 2.0‰; $n = 40$) from Nelson

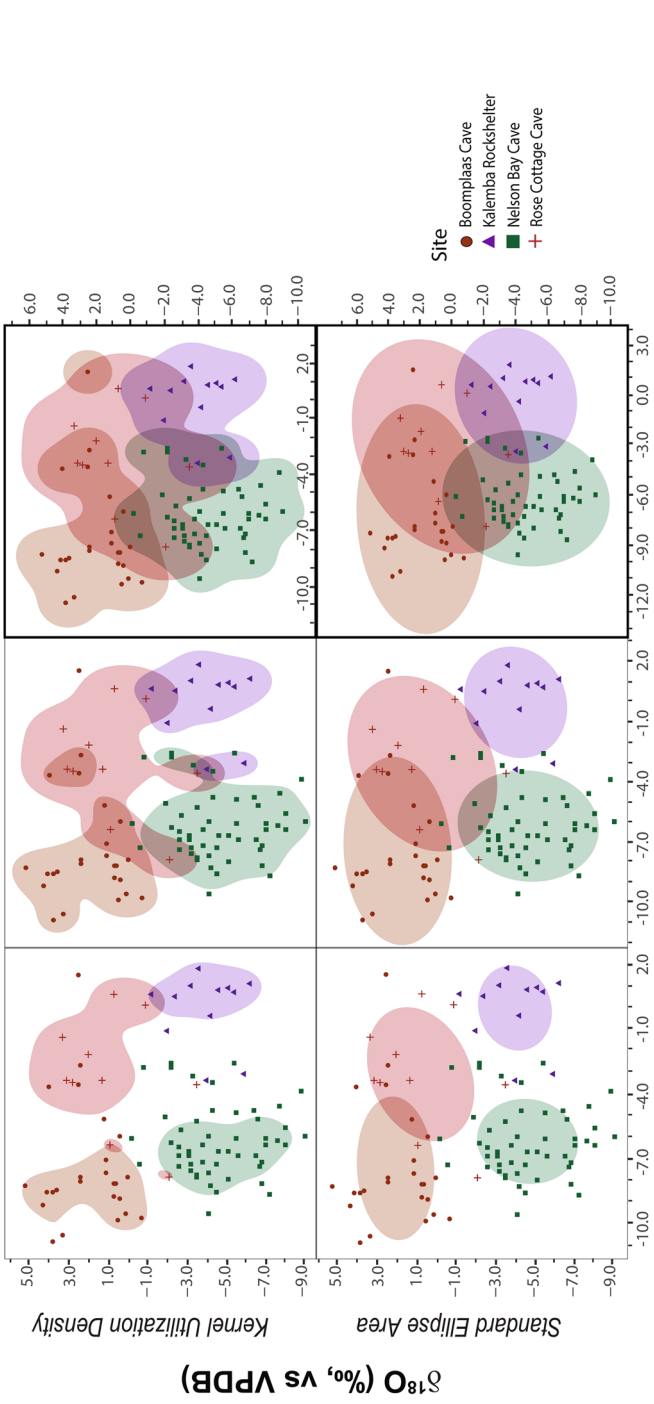

Fig. 4 Niche size and overlap for all grazer samples from individual study sites in the ~ 24,900–15,000-ya temporal bin. Rows represent different estimation methods (standard ellipse area (SEA) and kernel utilization density (KUD)). Columns display results at commonly selected contour levels of 50%, 75%, and 95%. In order to ensure that all plots present with equal proportions, the scales for the SEA and KUD methods at 95% differ. This is indicated by the thicker weight of the box boarder for these plots. VPDB, Vienna Pee Dee Belemnite

Table 5 Pair-wise isotopic niche overlaps from standard ellipse area (SEA) and kernel utilization density (KUD) for all grazers in the ~ 24,900–15,000-ya temporal bin

Method	Group	Boomplaas Cave			Nelson Bay Cave			Rose Cottage Cave			Kalemba Rockshelter		
		50%	*75%*	*95%*	*50%*	*75%*	*95%*	*50%*	*75%*	*95%*	*50%*	*75%*	*95%*
SEA	**BC**	–	–	–	0.00	0.00	*0.13*	*0.13*	*0.36*	*0.57*	0.00	0.00	0.00
	NBC	0.00	0.00	*0.17*	–	–	–	0.00	*0.14*	*0.44*	0.00	0.00	*0.12*
	RCC	*0.10*	*0.29*	*0.45*	0.00	*0.09*	*0.27*	–	–	–	0.00	*0.01*	*0.16*
	KR	0.00	0.00	0.00	0.00	0.00	*0.16*	0.00	*0.03*	*0.36*	–	–	–
KUD	**BC**	–	–	–	0.00	0.00	*0.10*	*0.01*	*0.33*	*0.55*	0.00	0.00	0.00
	NBC	0.00	0.00	*0.10*	–	–	–	0.00	*0.17*	*0.53*	0.00	*0.02*	*0.19*
	RCC	*0.01*	*0.19*	*0.35*	0.00	*0.11*	*0.36*	–	–	–	*0.02*	*0.10*	*0.23*
	KR	0.00	0.00	0.00	0.00	*0.03*	*0.29*	*0.05*	*0.23*	*0.51*	–	–	–

Overlaps provided at 50%, 75%, and 95% contour intervals. Italicized values indicate where overlap is estimated

Bay Cave have significantly lower $\delta^{18}O_{enamel}$ values than all study sites in this period (Tables S18–S20).

Approximately 10,900–5000 ya

Nelson Bay Cave occupies a very small area of isotope space in this temporal bin, a third of the size occupied by the same site in the ~ 24,900–15,000-ya bin and half the amount of area compared to the ~ 14,900–11,000-ya bin. Wonderwerk Cave occupies about three times the isotope space area of Nelson Bay Cave, followed by Rose Cottage Cave and Makwe Rockshelter. Tloutle occupies the most isotope space in this time period (Fig. 6; Table S38). Makwe Rockshelter isotope space is overlapped by Nelson Bay Cave at ~ 10%. The inverse relation, Nelson Bay Cave being overlapped by Makwe Rockshelter, occurs at a greater rate of ~ 40–85% at the 75% and 95% contours. Other overlaps with Nelson Bay Cave are estimated at < 5% at all intervals (Table 7). Rose Cottage Cave, Wonderwerk Cave, and Tloutle have varying degrees of overlap with each other at all contour levels. Makwe Rockshelter, Wonderwerk Cave, and Tloutle overlap each other at rates of ~ 10–20% at the 75% contour and ~ 30–40% at the 95% contour. Rose Cottage Cave and Makwe Rockshelter overlap ~ 10% or less and only at the 95% interval (Fig. 6; Table 7).

Grazers from Wonderwerk Cave (1.4 ± 1.5‰; $n = 100$) have the highest $\delta^{13}C_{enamel}$ values, significantly higher than those from any other site, in this temporal bin. Makwe Rockshelter (-0.8 ± 3.3‰; $n = 24$), Rose Cottage Cave (-2.0 ± 3.0‰; $n = 33$), and Tloutle (-2.7 ± 4.6‰; $n = 10$) have similar grazer $\delta^{13}C_{enamel}$ values to each other, but Rose Cottage Cave has higher grazer values than those from Nelson Bay Cave (-3.1 ± 1.3‰; $n = 9$) while the other two sites do not. Makwe Rockshelter has significantly higher grazer $\delta^{13}C_{enamel}$ values than a small sample from Kalemba Rockshelter

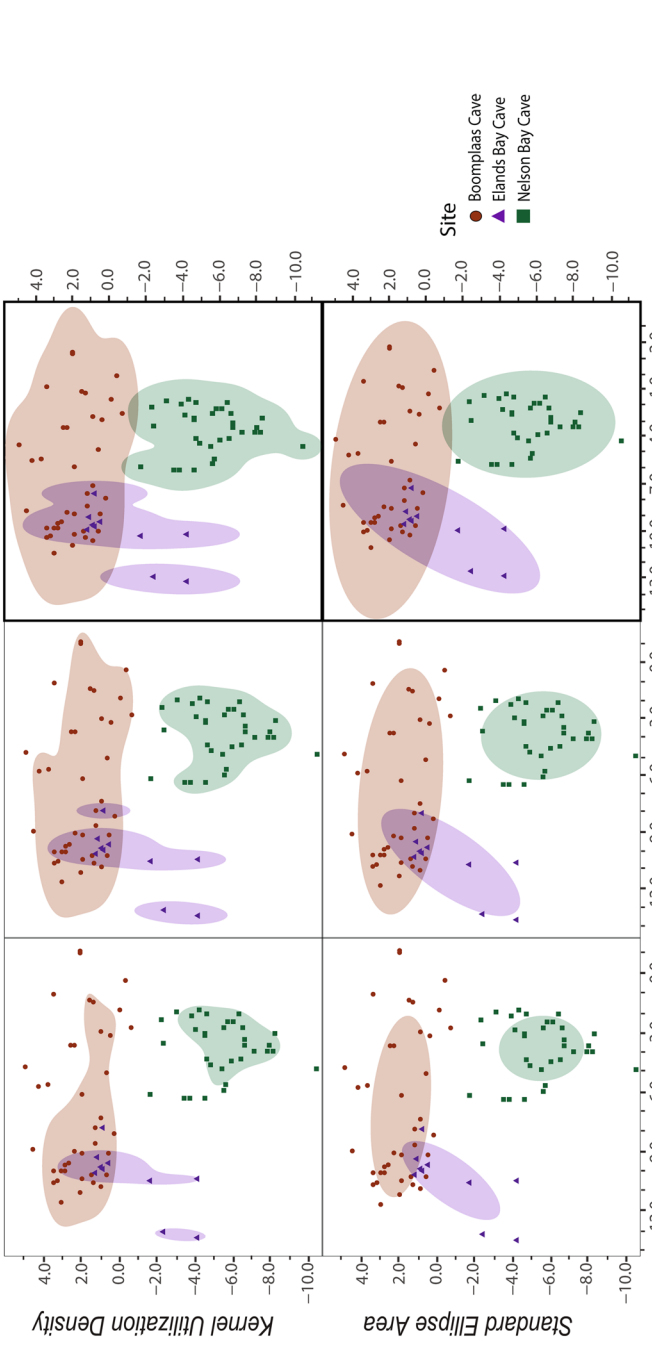

Fig. 5 Niche size and overlap for all grazer samples from individual study sites in the ~ 14,900–11,000-ya temporal bin. Rows represent different estimation methods (standard ellipse area (SEA) and kernel utilization density (KUD)). Columns display results at commonly selected contour levels of 50%, 75%, and 95%. In order to ensure that all plots present with equal proportions, the scales for the SEA and KUD methods at 95% differ. This is indicated by the thicker weight of the box boarder for these plots. VPDB, Vienna Pee Dee Belemnite

Table 6 Pair-wise isotopic niche overlaps from standard ellipse area (SEA) and kernel utilization density (KUD) for all grazers in the ~ 14,900–11,000-ya temporal bin

Method	Group	Boomplaas Cave			Sehonghong			Kalemba Rockshelter		
		50%	*75%*	*95%*	*50%*	*75%*	*95%*	*50%*	*75%*	*95%*
SEA	**BC**	–	–	–	*0.06*	*0.16*	*0.25*	0.00	0.00	*0.01*
	EBC	*0.12*	*0.32*	*0.50*	–	–	–	0.00	0.00	0.00
	NBC	0.00	0.00	*0.02*	0.00	0.00	0.00	–	–	–
KUD	**BC**	–	–	–	*0.15*	*0.15*	*0.19*	0.00	0.00	*0.01*
	EBC	*0.45*	*0.42*	*0.44*	–	–	–	0.00	0.00	0.00
	NBC	0.00	0.00	*0.02*	0.00	0.00	0.00	–	–	–

Overlaps provided at 50%, 75%, and 95% contour intervals. Italicized values indicate where overlap is estimated

($-5.4 \pm 3.3‰$; $n = 4$) which are estimated to have consumed ~ 45–50% of C_3 resources (Fig. S11; Tables S21–S23). Estimated C_3 consumption is < 30% by grazers from Nelson Bay Cave, Rose Cottage Cave, Tloutle, and Makwe Rockshelter and < 5% for grazers from Wonderwerk Cave. C_4-dominated diets are found for > 45% of grazers at Makwe Rockshelter, Rose Cottage Cave, and Tloutle, while Nelson Bay Cave, Rose Cottage Cave, and Kalemba Rockshelter have > 50% of grazers in the range $-8.0‰ \leq \delta^{13}C_{enamel}$ values $\leq -1.0‰$. Elands Bay Cave and Nelson Bay Cave are found to have 100% of grazers in that mixed-feeding category. C_3-dominated diets categorize > 20% of grazer samples from Tloutle and Kalemba Rockshelter (Fig. S3). Grazers from Rose Cottage Cave have the highest, and significantly different, $\delta^{18}O_{enamel}$ values, from all other sites. Wonderwerk Cave and Tloutle have similar grazer $\delta^{18}O_{enamel}$ values to each other, but significantly higher values than those from all other sites except Rose Cottage Cave. Kalemba and Makwe rockshelters also have similar $\delta^{18}O_{enamel}$ values. Nelson Bay Cave has the lowest grazer $\delta^{18}O_{enamel}$ values, significantly lower than those from any other site in this time bin (Tables S21–S23).

Approximately 4900–500 ya

Rose Cottage Cave occupies the smallest amount of isotope space of any site for any temporal bin, accounting for approximately one-eighth of the space occupied by this site compared with earlier time intervals. Wonderwerk Cave and Makwe Rockshelter are estimated to occupy slightly less isotope space in this period than in the ~ 10,900–5000-ya bin, with Makwe accounting for approximately double the isotope space of Wonderwerk (Table S39). Rose Cottage Cave isotope space is almost completely overlapped by Wonderwerk Cave (Fig. 7; Table 8). The inverse relationship finds an overlap of Wonderwerk Cave space by Rose Cottage Cave of ~ 20–25%. Makwe Rockshelter is found to overlap Rose Cottage Cave at the 75% and 95% contour intervals, but Rose Cottage Cave only overlaps Makwe Rockshelter space by ~ 5–10% at these same intervals. Makwe Rockshelter and Wonderwerk Cave are

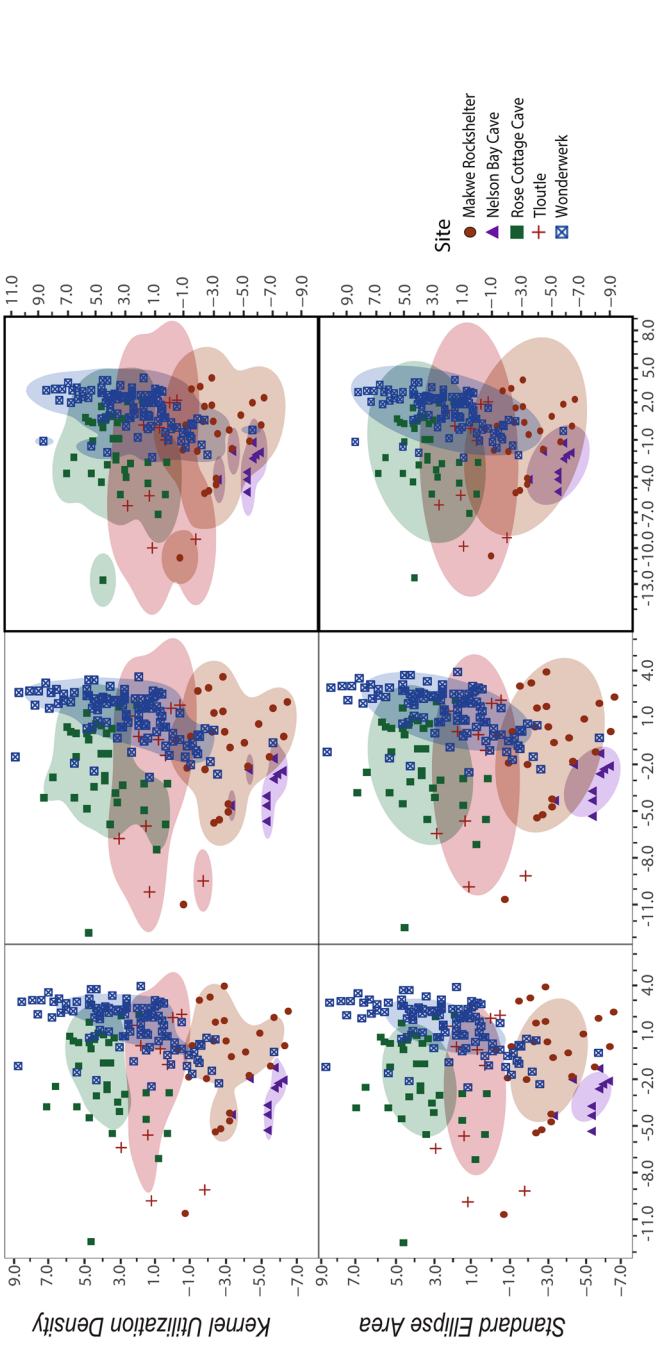

Fig. 6 Niche size and overlap for all grazer samples from individual study sites in the ~ 10,900–5000-ya temporal bin. Rows represent different estimation methods (standard ellipse area (SEA) and kernel utilization density (KUD)). Columns display results at commonly selected contour levels of 50%, 75%, and 95%. In order to ensure that all plots present with equal proportions, the scales for the SEA and KUD methods at 95% differ. This is indicated by the thicker weight of the box boarder for these plots. VPDB, Vienna Pee Dee Belemnite

Table 7 Pair-wise isotopic niche overlaps from standard ellipse area (SEA) and kernel utilization density (KUD) for all grazers in the ~ 10,900–5000-ya temporal bin

Method	Group	Nelson Bay Cave			Rose Cottage Cave			Wonderwerk			Tloutle			Makwe Rockshelter		
		50%	*75%*	*95%*	*50%*	*75%*	*95%*	*50%*	*75%*	*95%*	*50%*	*75%*	*95%*	*50%*	*75%*	*95%*
SEA	**NBC**	–	–	–	0.00	0.00	0.00	0.00	0.00	0.00	0.00	0.00	0.00	*0.01*	*0.44*	*0.87*
	RCC	0.00	0.00	0.00	–	–	–	*0.10*	*0.27*	*0.41*	*0.10*	*0.33*	*0.54*	0.00	0.00	*0.10*
	WC	0.00	0.00	0.00	*0.13*	*0.38*	*0.58*	–	–	–	*0.39*	*0.51*	*0.57*	0.00	*0.11*	*0.33*
	TL	0.00	0.00	0.00	*0.08*	*0.26*	*0.42*	*0.22*	*0.28*	*0.31*	–	–	–	0.00	*0.12*	*0.33*
	MR	0.00	*0.09*	*0.17*	0.00	0.00	*0.09*	0.00	*0.07*	*0.21*	0.00	*0.14*	*0.38*	–	–	–
KUD	**NBC**	–	–	–	0.00	0.00	0.00	0.00	0.00	*0.04*	0.00	0.00	0.00	0.00	*0.39*	*0.79*
	RCC	0.00	0.00	0.00	–	–	–	*0.16*	*0.23*	*0.43*	*0.01*	*0.40*	*0.54*	0.00	0.00	*0.06*
	WC	0.00	0.00	*0.01*	*0.21*	*0.32*	*0.54*	–	–	–	*0.53*	*0.55*	*0.53*	*0.01*	*0.19*	*0.34*
	TL	0.00	0.00	0.00	*0.01*	*0.27*	*0.39*	*0.26*	*0.27*	*0.30*	–	–	–	*0.01*	*0.10*	*0.30*
	MR	0.00	*0.05*	*0.11*	0.00	0.00	*0.05*	*0.01*	*0.12*	*0.26*	*0.01*	*0.13*	*0.41*	–	–	–

Overlaps provided at 50%, 75%, and 95% contour intervals. Italicized values indicate where overlap is estimated

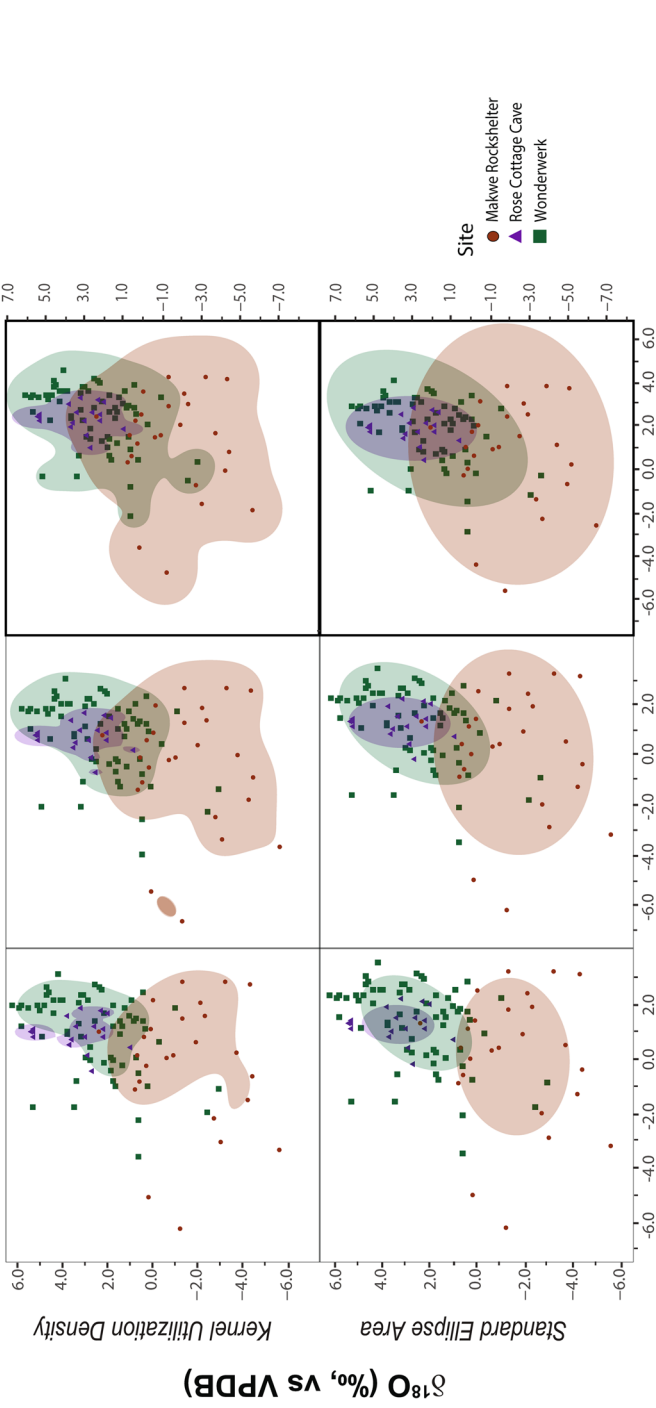

Fig. 7 Niche size and overlap for all grazer samples from individual study sites in the ~4900–500-ya temporal bin. Rows represent different estimation methods (standard ellipse area (SEA) and kernel utilization density (KUD)). Columns display results at commonly selected contour levels of 50%, 75%, and 95%. In order to ensure that all plots present with equal proportions, the scales for the SEA and KUD methods at 95% differ. This is indicated by the thicker weight of the box boarder for these plots. VPDB, Vienna Pee Dee Belemnite

Table 8 Pair-wise isotopic niche overlaps from standard ellipse area (SEA) and kernel utilization density (KUD) for all grazers in the ~ 4900–500-ya temporal bin

Method	Group	Rose Cottage Cave			Wonderwerk			Makwe Rockshelter		
		50%	*75%*	*95%*	*50%*	*75%*	*95%*	*50%*	*75%*	*95%*
SEA	**RCC**	–	–	–	*0.95*	*1.00*	*1.00*	0.00	*0.09*	*0.51*
	WC	*0.28*	*0.30*	*0.30*	–	–	–	*0.08*	*0.34*	*0.58*
	MR	0.00	*0.01*	*0.08*	*0.04*	*0.18*	*0.31*	–	–	–
KUD	**RCC**	–	–	–	*0.69*	*0.96*	*1.00*	*0.01*	*0.29*	*0.69*
	WC	*0.19*	*0.26*	*0.21*	–	–	–	*0.26*	*0.45*	*0.62*
	MR	0.00	*0.04*	*0.08*	*0.14*	*0.23*	*0.36*	–	–	–

Overlaps provided at 50%, 75%, and 95% contour intervals. Italicized values indicate where overlap is estimated

estimated to overlap each other at all contour levels, with greater overlap of Wonderwerk by Makwe than the reverse (Table 8).

Other sites are represented by fewer than nine grazer samples in this temporal bin, excluding them from isotope space analyses. Elands Bay Cave (-8.2 ± 0.8‰; $n = 7$) has significantly lower grazer $\delta^{13}C_{enamel}$ values than any other sites in this period. Nelson Bay Cave (-3.3 ± 0.5‰; $n = 4$) also has low grazer $\delta^{13}C_{enamel}$ values, significantly higher than those from Elands Bay Cave, but significantly lower than those from all other sites. Grazer values from Rose Cottage Cave (1.2 ± 0.6‰; $n = 18$) and Makwe Rockshelter (0.1 ± 2.5‰; $n = 25$) are similar. Wonderwerk Cave has the highest grazer $\delta^{13}C_{enamel}$ values (1.3 ± 1.5‰; $n = 66$), significantly higher than those from Makwe Rockshelter, but similar to those from Rose Cottage Cave (Fig. S12; Tables S24–S26). Estimated C_3 consumption by grazers is ~ 65–75% at Elands Bay Cave, ~ 30–35% at Nelson Bay Cave, and ~ 10% or less at Rose Cottage Cave, Wonderwerk Cave, and Makwe Rockshelter. All grazers from Rose Cottage Cave and Wonderwerk Cave, and ~ 75% from Makwe Rockshelter, have $\delta^{13}C_{enamel}$ values > -1.0‰, while all grazer samples from Nelson Bay Cave and > 50% from Elands Bay Cave have mixed-feeding $\delta^{13}C_{enamel}$ values. The remaining Elands Bay Cave grazers have $\delta^{13}C_{enamel}$ values < -8.0‰ (Fig. S3). $\delta^{18}O_{enamel}$ values among study sites are almost all significantly different. Rose Cottage Cave (3.5 ± 1.6‰; $n = 19$) has the highest $\delta^{18}O_{enamel}$ values and Nelson Bay Cave (-5.1 ± 1.6‰; $n = 19$) the lowest. Elands Bay Cave (0.9 ± 2.7‰; $n = 7$) and Makwe Rockshelter (-1.5 ± 2.0‰; $n = 25$) have similar $\delta^{18}O_{enamel}$ values, as do Rose Cottage Cave and Wonderwerk Cave (2.5 ± 2.0‰; $n = 66$; Tables S24–S26).

Discussion

Inferring Local Responses to Regional Climate Complexity

Elands Bay Cave, the one site found in the modern WRZ, has some of the smallest isotope space estimates and overlaps only with Boomplaas Cave (Tables 3 and

6). The size of isotope space occupied by Elands Bay Cave is driven by a contracted space on the $\delta^{13}C_{enamel}$ axis and an expanded space on the $\delta^{18}O_{enamel}$ axis (Figs. 2 and 5). This pattern is interpreted as indicating the source of precipitation coming from multiple sources under a different climate regime than today. Modern precipitation in the WRZ, and southwestern Africa in particular, is primarily driven by a combination of westerly wave cold fronts and southerly meridional flows bringing Atlantic moisture during the winter. Another source of precipitation over southern Africa, ridging South Atlantic anticyclones, has the potential to contribute moisture from the southwestern Indian Ocean, but is not a major source of precipitation for southwestern Africa in the present day (Diamond & Harris, 2019; Preston-Whyte & Tyson, 1988). Recent modeling, however, indicates that increased insolation would create a situation with greater precipitation over southwestern Africa attributable to ridging anticyclones (Ivanciu et al., 2022). It is anticipated that this precipitation with an increased contribution of moisture from the Indian Ocean would fall predominantly in winter (Ivanciu et al., 2022), although a ridging anticyclone has been implicated in extreme rainfall events in the Western Cape region during the summer of 1996 (Crimp & Mason, 1999). Based on analysis of speleothem records, Braun et al. (2019) argue that glacial precessional maxima (associated with increased solar insolation) causes a northward shift of the westerlies and an increase of Indian Ocean moisture over southern Africa during the Pleistocene. While speleothem records in that study did not extend into the latest Pleistocene to allow for a direct test during the LGM, the LGM is associated with precessional maxima at ~ 22 ka and modeling by Engelbrecht et al. (2019) indicates some increased rainfall over southwestern Africa in this period. The expanded $\delta^{18}O_{enamel}$ isotope space at Elands Bay Cave may be an indicator of moisture from the Indian Ocean contributing to winter rainfall over southwestern Africa. Narrow $\delta^{13}C_{enamel}$ space makes increased rainfall seasonality (i.e., more summer rain) unlikely as this would have resulted in expanded C_4 resources on the landscape which are not indicated at Elands Bay Cave. This follows from the dominance of C_3 fynbos vegetation in the WRZ (Cowling & Holmes, 1992; Vogel, 1978), with evidence for C_3 Poaceae grasses and Restionaceae plant varieties (Cordova, 2013).

In the two earliest time periods, little overlap is found for Boomplaas Cave and Sibhudu. Boomplaas is generally found to occupy less isotope space than Sibhudu, likely indicating greater winter rainfall during this period in the YRZ or Boomplaas Cave perhaps falling within an expanded WRZ (Figs. S5 and S6; Tables S31–S34). This is in general agreement with charcoal (Deacon, 1983; Deacon et al., 1984) and micromammal (Faith et al., 2019) analyses from Boomplaas Cave indicating increasing winter rainfall from ~ 60 ka to the LGM. Proxy data from further afield are more fragmentary for the period of and prior to the LGM, but Chase's (2010) synthesis of available data from archaeological sites concludes that MIS 4 (~ 74–58 ka) was relatively cool and moist compared to the present with increases in both summer and winter rainfall. Based on pollen percentages in marine core IODP U1479, the early MIS 4 period vegetation in southwestern Africa is dominated by forest and thicket with declining forest elements through later MIS 4 and MIS 3. At the same time, increased summer rainfall in southeastern Africa could result in lower $\delta^{18}O_{enamel}$

values at Sibhudu (Chase, 2021; Dupont et al., 2022; Engelbrecht et al., 2019). A shift to smaller isotope space in the ~ 49,900–36,000-ya temporal bin indicates a continuation and, perhaps, an intensification of cooler and drier conditions across southern Africa. This interpretation is supported by phytolith evidence for fynbos-dominated environments in the west (Esteban et al., 2020a) and a paleobotanical record from Waterfall Bluff in Eastern Cape Province indicating open woodlands with dry grasslands (Esteban et al., 2020b). Drier conditions are also suggested in late MIS 3 by charcoal peaks indicating burning at ~ 46–42 ka and ~ 33 ka (Quick et al., 2016) and the leaf wax record (Strobel et al., 2022) in the Vankervelsvlei wetland located in the YRZ. At Boomplaas Cave, micromammals indicate increasing aridity from ~ 50 to ~ 30 ka (Faith et al., 2019). Charcoal records from Boomplaas Cave (Deacon, 1983; Deacon et al., 1984) have recently been used to reconstruct temperature and precipitation for this time period. Temperatures are modeled to have decreased from ~ 44 to ~ 24 ka, but with a slight increase in precipitation at ~ 35 ka before a return to drier conditions (Khumalo, 2022). C_3-dominated environments and winter rainfall also characterize the Cango Caves speleothem in this time period (Talma & Vogel, 1992). The precipitation increase at ~ 35 ka modeled by Khumalo (2022) is likely related to a short period of warmer and wetter conditions from 39.7 to 36 cal BP in the BP stratigraphic unit, which is also seen in the site-specific stable isotope (Sealy et al., 2016) and micromammal (Avery, 2004) analyses from Boomplaas Cave. Regional analyses, like the current study or that of Faith et al. (2019), are, unfortunately, not temporally sensitive enough to capture local short-term changes like those in the BP unit.

YRZ sites, Boomplaas Cave and Nelson Bay Cave, are rarely found to overlap in isotope space, and Nelson Bay Cave is often estimated to have occupied less isotope space than Boomplaas Cave (Figs. 2 and 5; Tables 3 and 6). Even during periods of increased winter rainfall in southern Africa, the habitats around Nelson Bay Cave would have included more C_4 renosterveld and Karoo grasses than at Boomplaas Cave (Cordova, 2013; Rebelo et al., 2006). This is not to say that the environment around Nelson Bay Cave was dominated by C_4 grasslands, but that grazers in the LGM consumed some C_4 vegetation. This is a similar result to the site-specific isotope study (Sealy et al., 2020), although the isotope space measures indicate somewhat greater, as opposed to a similar amount, C_4 consumption by grazers at Nelson Bay Cave than at Boomplaas Cave. One possible explanation for this slight difference in C_4 consumption at Nelson Bay Cave may be the availability of C_4-dominated grasslands in the eastern PAP as modeled by Cowling et al. (2020); however, strontium isotope analyses have not provided convincing evidence of seasonal migrations by grazing fauna (Copeland et al., 2016; Lehmann et al., 2018).

In the ~ 35,900–25,000-ka temporal bin, Boomplaas Cave and Sehonghong nearly completely overlap with expansion along the $\delta^{18}O_{enamel}$ axis and contraction on the $\delta^{13}C_{enamel}$ axis (Fig. 3). MIS 3 conditions across southern Africa are complex and varied (Knight & Fitchett, 2021), but both locations appear to be characterized by increased winter rainfall and C_3-dominated, including C_3 grass–dominated, environments. Micromammals from Boomplaas Cave indicate an LGM with enhanced winter rainfall (Faith et al., 2019), and environmental modeling of charcoal from the site identifies the coolest and driest parts of the sequence at ~ 24 ka (Khumalo,

2022). Charcoal and pollen analysis reveals a plant community characterized by low diversity and dominated by shrubs of the *Elytropappus*/*Stoebe* group, which is present today in marginal areas between karoo and fynbos (Deacon & Lancaster, 1988; Deacon et al., 1984; Scott, 1989). Furthermore, the LGM is characterized by a $\delta^{13}C$ minimum in the Cango Caves speleothem which has been interpreted as a nearly complete C_3 environment (Talma & Vogel, 1992). Further afield at Pinnacle Point, speleothem records indicate a shift to increasing winter rainfall conditions and a dominance of C_3 vegetation (Bar-Matthews et al., 2010; Braun et al., 2019), while phytolith records from PP5-6 indicate open fynbos conditions with an abundance of C_3 grasses (Esteban et al., 2020a) in MIS 3. $\delta^{13}C$ of soil organic matter (SOM) from the sites of Sehonghong (Loftus et al., 2015), Ha Makotoko, and Ntloana Tsoana (Roberts et al., 2013) indicates that late Pleistocene vegetation from about ~ 35 ka to the Holocene boundary was dominated by C_3 plants in the Lesotho highlands. The Sehonghong results indicate a major altitudinal decline in C_3 grasses as the site is located at ~ 1870 m above sea level well below the transition with C_4 species extending up to 2700 m on north-facing slopes or to about 2100 m on south-facing slopes today (Parker et al., 2011). Lower $\delta^{18}O_{enamel}$ values at Sehonghong than those at the other Lesotho sites in the post-LGM period may suggest a different source of precipitation in the ~ 35,900–25,000-ya bin, perhaps an increase in the WRZ and expansion of the YRZ into Lesotho as modeled by van Zinderen Bakker (1967, 1976) and Cockcroft et al., (1987; see also Stewart & Mitchell, 2018). This would indicate a shift away from or a decrease in importance of the current pattern of rainfall over Lesotho which is primarily a result of the uplift of moist Indian Ocean air in the summer (Loftus et al., 2015; Tyson & Preston-Whyte, 2000).

Boomplaas Cave isotope space decreases through time from ~ 70,000 to ~ 25,000 ya at which point it quadruples in area by ~ 14,900–11,000 ya, and, at more recent periods, is often found to be overlapping with Rose Cottage Cave (Tables S31, S33, and S35–S37). The similarities among these sites may be related to changing rainfall seasonality through time, particularly in the latest Pleistocene and earliest Holocene. These patterns in shifting isotope space at Boomplaas Cave capture the increase in winter rainfall and dominance of C_3 grasslands earlier in the sequence, and the shift to more summer rainfall and expanding C_4 grasses after the LGM and into the Holocene. Contracting isotope space, particularly along the $\delta^{18}O_{enamel}$ axis, is interpreted here as indicating a single source or single season–dominated rainfall (Fig. 4). It is not suggested here that Boomplaas Cave and Rose Cottage Cave received precipitation from the same source, but, instead, that these sites experienced a greater portion of summer rainfall in the period after ~ 14 ka than earlier in the Pleistocene. At Boomplaas Cave, this is consistent with an increase in summer rainfall interpreted from the micromammal assemblage starting ~ 16 ka (Faith et al., 2019), evidence for mountain woodland taxa which prefer moist and warm conditions in the pollen record at ~ 15 ka (Scott, 1989), and the highest modeled rates of precipitation from the charcoal record between ~ 16 and ~ 11 ka (Khumalo, 2022). Similarly, the Cango Caves speleothem record has higher $\delta^{13}C$ values and, to a lesser extent, higher $\delta^{18}O$ values, indicating more C_4 grasses and increasing summer rainfall at this time (Talma & Vogel, 1992). On a regional scale, climate modeling has indicated that Northern Hemisphere glaciation, particularly during the LGM and the subsequent

period, resulted in wetter conditions throughout southern Africa (Engelbrecht et al., 2019). Paleoclimatic records from Wonderwerk Cave (Brook et al., 2010) and a pollen record from the Wonderkrater spring (Scott et al., 2003) indicate wetter conditions from ~ 23–17 ka. A recent compilation and analysis of large mammal fauna also suggests that the currently arid interior of southern African may have experienced more mesic conditions during the LGM and post-LGM periods (Reynard, 2021). Over the same time period, the $\delta^{13}C_{enamel}$ axis expands at Boomplaas Cave and Rose Cottage Cave (Figs. 4, 5, and 6). This may indicate an increasing variety of available grassy vegetation, as is also suggested in the Cango Caves speleothem (Talma & Vogel, 1992). Increased summer rainfall and decreased seasonality at maximum precession are interpreted to have been conducive to forest and thicket vegetation growth which would have supported a heterogeneous grass community (Dupont et al., 2022) and may help explain the presence of woody taxa in the Boomplaas Cave pollen record (Scott, 1989).

Similar to Elands Bay Cave, Nelson Bay Cave isotope space is rarely found to be overlapped, and when it is, primarily indicated at the 75% and 95% contour levels, it is, unexpectedly, by the Zambian sites of Kalemba and Makwe rockshelters (Tables 3, 5, and 7). The difference between Boomplaas Cave and Nelson Bay Cave has previously been identified by Sealy and colleagues (2020), but the stark isotope space differences add additional support for environmental heterogeneity within the YRZ. Similarities in isotope space between Nelson Bay Cave and the Zambian sites, particularly Makwe Rockshelter, are largely driven by Nelson Bay Cave's small isotope space area being nearly completely overlapped by the much larger isotope spaces of Kalemba and Makwe. This may suggest similarities in terms of the presence of C_4 grasses at these sites in the latest Pleistocene and earliest Holocene, but the much larger isotope space along the $\delta^{13}C_{enamel}$ axis at the Zambian sites indicates a dominance of C_4 vegetation (Table S40) that is not supported by the record at Nelson Bay Cave. The small isotope space occupied by Nelson Bay Cave suggests low diversity in the environment at this time period. In conjunction with sea level changes, renosterveld floral communities may have moved further east beyond modern-day Port Elizabeth, although the dynamics of these paleolandscapes continue to be investigated (Cleghorn et al., 2020; Marean et al., 2020; Ward et al., 2022). Therefore, the very constricted isotope space occupied by Nelson Bay Cave in the ~ 10,900–5000-ya temporal bin (Fig. 6) may be a result of sea level rise and the disappearance of the PAP (Jerardino, 2022; Jerardino et al., 2018), but more work is needed to characterize the specifics of this habitat and its relationship to shifting coastlines and sea levels in the latest Pleistocene and earliest Holocene. In the Zambezi Basin, there is evidence for greater rainfall during the LGM and the terminal Pleistocene-Holocene transition associated with the Younger Dryas (Dupont & Kuhlmann, 2017; Wang et al., 2013), perhaps as a result of the southward movement of the Central African rain belt due to increased glaciation in the Northern Hemisphere at this time (Chase, 2021). As a result, the similar isotope space signatures from these two regions may only be indicating superficial similarities as opposed to some sort of regionally driven environmental regime.

Interior sites are found to overlap in various combinations throughout the timeframe of this study. In the ~ 24,900–15,000-ya temporal bin, Kalemba Rockshelter

and Rose Cottage Cave do not overlap at all, likely indicating different environmental conditions at these sites (Fig. 4; Table 5). As previously mentioned, climatic conditions further north in the Zambezi Basin have an opposing response to widespread drier conditions in southern Africa with wetter conditions indicated throughout this period (Chase, 2021). Interior sites are not represented by the isotope space metrics in the ~ 14,900–11,000-ya period due to small samples of grazers, but Wonderwerk Cave and Equus Cave have the highest $\delta^{13}C_{enamel}$ values of this time period, significantly higher than those from most other sites (Tables S18–S20).

With the return of the African rain belt northward, $\delta^{13}C_{enamel}$ values at Kalemba Rockshelter are lower and $\delta^{18}O_{enamel}$ values are higher in the ~ 10,900–5000-ya bin (Fig. 6; Table S21). This coincides with evidence for greater C_3 resource consumption by grazers, specifically equids, at Equus Cave and Kalemba Rockshelter at ~ 10,000 ya (Lee-Thorp & Beaumont, 1995; Robinson, 2017) and broader C_3 grasslands in southern Africa at the time (Breman et al., 2019). Some widespread similarity of interior sites is indicated in the ~ 10,900–5000-ya temporal bin with overlap of isotope space measured between Rose Cottage Cave and Wonderwerk Cave and between Wonderwerk Cave and Makwe Rockshelter (Table 7). Rose Cottage Cave occupies a very small amount of isotope space in the ~ 4900–500-ya period with some overlap by Wonderwerk Cave, but not Makwe Rockshelter. Wonderwerk Cave and Makwe Rockshelter, which overlap each other in isotope space, both indicate a constricted isotope space in this final temporal bin compared with the previous one at ~ 10,900–5000 ya (Fig. 7; Tables S38 and S39). $\delta^{13}C_{enamel}$ values from Ha Makotoko, Ntloana Tsoana, and Tloutle, despite small sample sizes and likely non-representative samples, are always lower than those from Rose Cottage Cave, likely reflecting their higher elevation at ~ 1870 m versus ~ 1600 m for Rose Cottage and, as such, a greater portion of C_3 grasses (Tables S21–S26). The isotope space and overlap patterns of these two temporal bins reflect the complex nature of Holocene climate patterns. Overall higher $\delta^{18}O_{enamel}$ values in this time period may be related to mid-Holocene aridity with a particularly strong effect at higher altitude sites like Rose Cottage Cave. Long-term research in the southwestern Cape near Elands Bay Cave has identified two major hot and arid events: the mid-Holocene antithermal (~ 8200–4200 ya) and the Medieval warm epoch (~ 1300–650 ya; Jerardino et al., 2018; Jerardino, 2022; Herbert & Fitchett, 2022). These phases are interspersed by cooler and wetter periods at ~ 4200 ya and from ~ 2500 to 1800 ya (Jerardino, 1995; Jerardino et al., 2018). Pollen records from the Limpopo Basin (Dupont et al., 2011), the continental interior (Chase et al., 2015a), and the Cederberg Mountains of the southwestern Cape (Chase et al., 2015b) provide evidence for more humid conditions during the terminal Pleistocene and early Holocene which can be attributed to summer rainfall increases prior to ~ 8000 ya. Records from interior sites like Florisbad (Scott & Nyakale, 2002), Wonderwerk (Brook et al., 2010), and Cold Air Cave (Holmgren et al., 2003) indicate increasingly arid conditions through the mid-Holocene with only brief intervals of higher moisture availability. This may be reflected in the pattern along the $\delta^{18}O_{enamel}$ axis where Rose Cottage Cave, Wonderwerk Cave, and Makwe Rockshelter all have narrow, but mostly non-overlapping values (Fig. 6). Such a result may be explained by shifts in rainfall seasonality, but as a result of different climate patterns in the interior versus the Lesotho highlands.

In Zambia, the retreat of Northern Hemisphere glaciers would have contributed to these more arid conditions in the Holocene as the Central African rain belt returned northwards (Chase, 2021). The shifting nature of the ITCZ and the Central African rain belt may also explain changes in rainfall at Wonderwerk Cave. At Wonderwerk Cave, the isotope space measures actually reveal expansion along the $\delta^{18}O_{enamel}$ axis (Figs. 6 and 7). This may indicate temporal mixing related to periods of more or less aridity and the starting isotopic composition of source precipitation shifting from the latest Pleistocene into the Holocene. Engelbrecht et al. (2019) identify an increase in summer rainfall over the central interior region of South Africa during glacial periods and tentatively attribute it to the southward displacement of tropical-temperate trough formation. The northward return of these rain belts in the Holocene would have reduced overall precipitation in the central interior, becoming most evident in the middle and late Holocene. Rainfall for the central interior would return to being dominated by advection of Agulhas water, and the wide range of $\delta^{18}O_{enamel}$ values at Wonderwerk Cave may be partially explained by the loss of ^{16}O during inland transport of source moisture. Higher $\delta^{18}O_{enamel}$ values at Rose Cottage Cave are likely the result of a different climatic change, such as a decrease in winter rainfall. Source precipitation at Rose Cottage Cave during this time may be from minor northward latitudinal shifts in frontal systems as climate regimes began to settle into present-day patterns (Jerardino, 1995). Down-scaled climate models indicate less winter precipitation in Lesotho under current climate regimes than during periods of glacial ice cover (Engelbrecht et al., 2019). Combined with evidence that winter rainfall tends to have lower $\delta^{18}O$ values (Diamond & Harris, 2019; Harris et al., 2010), this could explain the constricting isotope space at Rose Cottage Cave in the Holocene. Furthermore, this may indicate that Rose Cottage Cave was occupied during warmer and drier periods in the Holocene, and not at times when cooler and wetter conditions are thought to have led to Neoglacial altitudinal expansions of C_3 grasses in the region. For instance, phytolith analysis from Likoaeng at ~ 1725 m in the Senqu Valley of Lesotho indicates an expansion of C_3 grasses from ~ 2900 to 2100 cal BP (Parker et al., 2011) in accordance with models developed by Jerardino (1993, 1995), but there are few archaeological remains from this period at Rose Cottage Cave (Loftus et al., 2019; Wadley, 1991, 1996, 1997, 2000, 2001).

"On the ground" analyses of environments through isotope space measures appear to capture many of the major late Pleistocene and Holocene climatic trends based on off-shore records, speleothem datasets, and regional models (Carr et al., 2016; Chase, 2021; Cleghorn et al., 2020; Dupont et al., 2022; Stratford et al., 2021), but also reveal sub-regional differences that may have been crucial drivers of human interactions and in the development of human behaviors and technologies. While there appears to be some differentiation based on environmental zone, there are many examples of sites within an environmental zone not having overlapping isotope space and, instead, overlapping with sites in other environmental zones. As a result, the first hypothesis that sites within an environmental zone would have largely similar and overlapping isotope space must be rejected, with the implication being that there is greater intra-regional environmental heterogeneity than expected. That said, the isotope space approach does reveal that there are some regional trends and not that every site is characterized by its own specific environmental context.

There is much more support for the second hypothesis that patterns of contracting and expanding isotope space are an indicator of seasonality and, perhaps, source of rainfall. Contraction along the $\delta^{18}O_{enamel}$ axis paired with expansion along the $\delta^{13}C_{enamel}$ axis resulting in an overall expansion of isotope space appears to indicate a shift to single-season, usually summer-dominated, rainfall. Under these conditions, a wider variety of grassy vegetation may be available (Cowling & Holmes, 1992; Vogel, 1978), suggesting an environmental change. While contraction and expansion of isotope space may indicate other events, such as rising sea levels and the loss of the PAP at Nelson Bay Cave over time, I tentatively accept the second hypothesis that isotope space measures are a useful tool for characterizing rainfall seasonality with the recognition that more work, including establishing modern analogs and baselines, is required before full acceptance.

Future Directions

Faunal stable isotope analyses are only one part of the picture when trying to reconstruct the environmental conditions experienced by human populations and the circumstances of those conditions at different spatial scales from the broader region down to the local site. For instance, the current study finds greater differences in local conditions among southern African sites than does a compilation of large mammal remains from many of these same sites (Reynard, 2021). Further development of multi-site databases of environmental proxies is likely to reveal additional aspects of local paleoenvironments and clarify some of the oversimplifications resulting from stable isotope data. For example, while we can assume that changes in grazer $\delta^{13}C_{enamel}$ values reflect different proportions of C_3 and C_4 grasses in the diet, proxies like mesowear scores (Sealy et al., 2020) can provide insight to the types of C_3 and C_4 vegetation consumed but are currently only widely available for a few sites. Including analyses like mesowear or microwear could allow individual specimens to be identified as grazers or browsers, avoiding the use of taxonomic uniformitarianism in establishing dietary categories which may obscure crucial paleoenvironmental patterns. Pollen, phytolith, and charcoal records also exist for many southern African archaeological sites (Bamford, 2021; Stratford et al., 2021) and await a thorough multi-site analysis.

Considerable potential exists for expanding local faunal stable isotope datasets as well. Despite the current study demonstrating the rich and nuanced environmental details that can be distilled from ~ 1200 stable isotope samples across 13 study sites, this represents only ~ 5% of the known cave and rockshelter sites in southern Africa (Stratford et al., 2021), and none of the open-air sites of the interior (Wilkins, 2021). Returning to the already collected and curated collections for many of these sites offers the promise of filling in gaps in our current understanding of site-level environments and how regional climatic patterns are manifested locally. It is also important to reinvestigate some of the sites included in this study, in particular, those in Lesotho. Stewart & Mitchell (2018) have produced a thorough paleoecological framework for the Maloti-Drakensberg region, but because of the sparse samples from sites like Ha Makotoko, Ntloana Tsoana, and Tloutle, and

the temporally restricted collection from Sehonghong, it is not possible to conduct a meaningful comparison. Expanding these datasets to include additional species and time periods will allow for finer analysis of the habitats and environments in this region and stronger reconstructions to compare with other sites in southern Africa.

More thought and work are also needed to understand the process and purpose of adjusting $\delta^{13}C_{enamel}$ values for changes in atmospheric $\delta^{13}C$ values of individual samples or specific temporal periods. As Sealy et al. (2020) demonstrate, not adjusting values, or simply adjusting all samples by a single standard factor to compare with modern fauna, misses crucial differences in C_3 and C_4 consumption within and across archaeological sites during the late Pleistocene and Holocene. In the current study, the statistical comparisons of $\delta^{13}C_{enamel}$ values within and among sites almost all have the same results whether unadjusted or adjusted values are used (see Supplementary Discussion in Online Resource 2); so, is adjusting $\delta^{13}C_{enamel}$ values always necessary? Consensus is also needed in terms of which values to use for endmembers, what date to use as "modern" or "current," and how to deal with differences among sites in chronological quality and resolution. These factors may partially explain why some sites are found to have statistically significantly different adjusted $\delta^{13}C_{enamel}$ values compared with unadjusted values, while other sites, even in the same temporal bin, do not, although physiological and climatological aspects may also be at play.

Finally, more comprehensive modern enamel stable isotope datasets with paired environmental information, similar to research by Luyt et al. (2019) in the WRZ, are required to develop models and baselines for comparing and interpreting the patterns we see in the archaeological record when conducting isotope space and overlap analyses. While the current approach appears to help identify changes in rainfall seasonality, establishing whether the relationship between contracting and expanding isotope space on different axes holds up across modern ecosystems would increase the confidence that it reflects real changes in precipitation of the past. Relatedly, we need to establish critical isotope space thresholds for determining shifts in rainfall seasonality. A further consideration would be to address the efficacy of combining enamel stable isotope data generated by different laboratories (e.g., Pestle et al., 2014) for meta-analyses such as the one conducted here. Are there correction factors, minimum meaningful differences, or other issues we need to consider and control for in our regional compilations? Careful consideration of each of these factors will ultimately allow for better analyses that result in more accurate and refined paleoenvironmental reconstructions.

Conclusion

As researchers increasingly turn towards modeling approaches in attempts to reconstruct late Pleistocene and Holocene exchange and social networks, the thorough integration and multi-site analysis of local paleoecological datasets will be critical assets in model refinement and functionality. In southern Africa, faunal enamel stable isotope analysis has only been conducted at a small percentage of

sites, but it is an important source of site-level, on-the-ground, environmental and habitat conditions. While these sites have been investigated individually, or as a small group in the case of some sites from Lesotho, compiling a multi-site database and treating each site in the same way with radiocarbon calibration have allowed for explicit hypothesis testing of the local manifestations of regional climatic conditions through the relatively new approach of isotope space measures. Isotope space and overlap analyses indicate greater intra-regional environmental heterogeneity than expected, but also reveal a potentially useful pattern of contracting and expanding isotope space that can be used to indicate seasonality of rainfall. It is clear that our ancestors experienced varied ecological conditions in southern Africa during the late Pleistocene and Holocene that likely affected their technology, material culture, and social systems. While stable isotope data identifies more nuanced on the ground environmental circumstances in southern Africa than analysis of the large fauna alone (Reynard, 2021), even further knowledge may be derived from synthesizing and integrating other lines of site-level paleoecological data. Incorporating local habitat conditions into models of human movement and interaction on a site-by-site basis holds the potential to reveal deeper insights to the development of MSA and LSA behaviors and demographic patterns.

Supplementary Information The online version contains supplementary material available at https://doi.org/10.1007/s41982-023-00160-0.

Acknowledgements Stable isotope characterization of the Kalemba and Makwe rockshelter fauna was supported by a National Science Foundation Archaeology Doctoral Dissertation Improvement Grant (BCS – 1245803) to J.R.R. and Dietrich W. Stout. Research and export permits in Zambia were issued by the National Heritage Conservation Commission and the National Museums Board of Zambia (awarded 16 May 2013). I thank Terry Nyambe, Maambo Bwanjelela, and Chipo Simunchembu for access to the archaeological collections of the Livingstone Museum, and Taisa Kamwi and MacMillon Mudenda with the National Heritage Conservation Commission for their support in the research and export permitting process. Characterization of samples from Sibhudu was supported by a Rust Family Foundation Research Grant (RFF-2017-31). The Rust Family Foundation played no role in the study design; collection, analysis, and interpretation of the data, or writing of this manuscript. Sampling and export permissions for the Sibhudu material were granted by a permit (#1899) from the South African Heritage Resources Agency (SAHRA). I thank Lyn Wadley for her support and permission to access and sample the Sibhudu material in the Evolutionary Studies Institute at the University of the Witwatersrand. Stable isotope sample preparation and characterization were performed with the assistance of John Krigbaum and Jason Curtis in the Department of Anthropology and Department of Geosciences and the Light Stable Isotope Laboratory at the University of Florida. I thank the three anonymous reviewers who provided thoughtful and insightful comments on the initial draft of this manuscript, helping craft it into a stronger contribution. I also thank Teresa Steele for being the handling editor of this manuscript and for prompt replies and guidance throughout the submission process. Finally, I wish to thank the many researchers who have worked at the study sites and analyzed the zooarchaeological collections from these sites. Without the years of work of those researchers, multi-site compilation studies such as this one would not be possible.

Author Contribution Not applicable. The sole author, J.R.R., completed all compilations, analyses, and writing of the manuscript.

Funding New data presented here from Kalemba and Makwe rockshelters were supported by a National Science Foundation Archaeology Doctoral Dissertation Improvement Grant (BCS – 1245803) to J.R.R. and Dietrich W. Stout. New data from Sibhudu were supported by a Rust Family Foundation Research Grant (RFF-2017–31).

Data Availability The dataset compiled and analyzed during the current study are included in this published article and its supplementary online resources.

Declarations

Ethical Approval Not applicable.

Competing Interests The author declares no competing interests.

References

Ambrose, S. H., & DeNiro, M. J. (1986). The isotopic ecology of East African mammals. *Oecologia, 69*(3), 395–406.

Ames, C. J., Gliganic, L. A., Cordova, C., Boyd, K., Jones, B. G., Maher, L., & Collins, B. (2020). Chronostratigraphy, site formation, and palaeoenvironmental context of late Pleistocene and Holocene occupations at Grassridge rock shelter (Eastern Cape, South Africa). *Open Quaternary, 6*(1), 1–19.

Avery, D. M. (2004). Size variation in the common molerat *Cryptomys hottentotus* from Southern Africa and its potential for palaeoenvironmental reconstruction. *Journal of Archaeological Science, 31*(3), 273–282.

Backwell, L. R., McCarthy, T. S., Wadley, L., Henderson, Z., Steininger, C. M., Deklerk, B., Barré, M., Lamothe, M., Chase, B. M., Woodborne, S., & Susino, G. J. (2014). Multiproxy record of late Quaternary climate change and Middle Stone Age human occupation at Wonderkrater, South Africa. *Quaternary Science Reviews, 99*, 42–59.

Bamford, M. K. (2021). Pollen, charcoal and phytolith records from the Late Quaternary of Southern Africa: Vegetation and climate interpretations. *South African Journal of Geology 2021, 124*(4), 1047–1054.

Bar-Matthews, M., Marean, C. W., Jacobs, Z., Yaryanas, P., Fisher, E. C., Herries, A. I. R., Brown, K., Williams, H. M., Bernatchez, J., Ayalon, A., & Nilssen, P. J. (2010). A high resolution and continuous isotopic speleothem record of paleoclimate and paleoenvironment from 90 to 53 ya from Pinnacle Point on the south coast of South Africa. *Quaternary Science Reviews, 29*(17–18), 2131–2145.

Baumann, C., Hussain, S. T., Roblíčková, M., Riede, F., Mannino, M. A., & Bocherens, H. (2023). Evidence for hunter-gatherer impacts on raven diet and ecology in the Gravettian of Southern Moravia. *Nature Ecology & Evolution, 7*, 1302–1314.

Beaumont, P. B., Miller, G. H., & Vogel, J. C. (1992). Contemplating old clues to the impact of future greenhouse climates in South Africa. *South African Journal of Science, 88*(9–10), 490–498.

Beyer, R. M., Krapp, M., Eriksson, A., & Manica, A. (2021). Climatic windows for human migration out of Africa in the past 300,000 years. *Nature Communications, 12*(1), 1–10.

Blome, M. W., Cohen, A. S., Tryon, C. A., Brooks, A. S., & Russell, J. (2012). The environmental context for the origins of modern human diversity: A synthesis of regional variability in African climate 150,000–30,000 years ago. *Journal of Human Evolution, 62*(5), 563–592.

Blumenthal, S. A., Levin, N. E., Brown, F. H., Brugal, J. P., Chritz, K. L., Harris, J. M., Jehle, G. E., & Cerling, T. E. (2017). Aridity and hominin environments. *Proceedings of the National Academy of Sciences, 114*(28), 7331–7336.

Bousman, C. B., & Brink, J. S. (2018). The emergence, spread, and termination of the Early Later Stone Age event in South Africa and southern Namibia. *Quaternary International, 495*, 116–135.

Braun, K., Bar-Matthews, M., Matthews, A., Ayalon, A., Cowling, R. M., Yaryanas, P., Fisher, E. C., Dyez, K., Zilberman, T., & Marean, C. W. (2019). Late Pleistocene records of speleothem stable isotopic compositions from Pinnacle Point on the South African south coast. *Quaternary Research, 91*(1), 265–288.

Breman, E., Ekblom, A., Gillson, L., & Norström, E. (2019). Phytolith-based environmental reconstruction from an altitudinal gradient in Mpumalanga, South Africa, 10,600 BP–present. *Review of Palaeobotany and Palynology, 263*, 104–116.

Brink, J. S. (1999). Preliminary report on a caprine from the Cape mountains, South Africa. *Archaeozoologia, 10*, 11–26.

Bronk Ramsey, C. (2009). Bayesian analysis of radiocarbon dates. *Radiocarbon, 51*(1), 337–360.

Brook, G. A., Scott, L., Railsback, L. B., & Goddard, E. A. (2010). A 35 ka pollen and isotope record of environmental change along the southern margin of the Kalahari from a stalagmite and animal dung deposits in Wonderwerk Cave, South Africa. *Journal of Arid Environments, 74*(7), 870–884.

Carr, A., Chase, B. M., & Mackay, A. (2016). Mid to Late Quaternary landscape and environmental dynamics in the Middle Stone Age of southern South Africa. In S. Jones & B. Stewart (Eds.), *Africa from MIS 6–2* (pp. 23–47). Springer.

Carr, A. S., Chase, B. M., Birkinshaw, S. J., Holmes, P. J., Rabumbulu, M., & Stewart, B. A. (2023). Paleolakes and socioecological implications of last glacial "greening" of the South African interior. *Proceedings of the National Academy of Sciences, 120*(21), e2221082120.

Cawthra, H. C., Cowling, R. M., Andò, S., & Marean, C. W. (2020). Geological and soil maps of the Palaeo-Agulhas Plain for the Last Glacial Maximum. *Quaternary Science Reviews, 235*, 105858.

Cerling, T. E., Harris, J. M., & Passey, B. H. (2003). Diets of East African Bovidae based on stable isotope analysis. *Journal of Mammalogy, 84*(2), 456–470.

Cerling, T. E., Harris, J. M., Hart, J., Yaleme, P., Klingel, H., Leakey, M. G., Levin, N. E., & Passey, B. H. (2008). Stable isotope ecology of the common hippopotamus. *Journal of Zoology, 276*(2), 204–212.

Cerling, T. E., Andanje, S. A., Blumenthal, S. A., Brown, F. H., Chritz, K. L., Harris, J. M., Hart, J. A., Kirera, F. M., Yaleme, P., Leakey, L. N., Leakey, M. G., Levin, N. E., Manthi, F. K., Passey, B. H., & Uno, K. T. (2015). Dietary changes of large herbivores in the Turyana Basin, Kenya from 4 to 1 million years ago. *Proceedings of the National Academy of Sciences, 112*, 11467–11472.

Cerling T. E. (2014). Stable isotope evidence for hominin environments in Africa. In: Cerling, T. E. (ed.) *Treatise on geochemistry. Vol. 14: Archaeology and anthropology*. Oxford, UK: Springer, pp. 158–166.

Chase, B. (2009). Evaluating the use of dune sediments as a proxy for palaeo-aridity: A Southern African case study. *Earth-Science Reviews, 93*(1–2), 31–45.

Chase, B. M. (2010). South African palaeoenvironments during marine oxygen isotope stage 4: A context for the Howiesons Poort and Still Bay industries. *Journal of Archaeological Science, 37*(6), 1359–1366.

Chase, B. M. (2021). Orbital forcing in Southern Africa: Towards a conceptual model for predicting deep time environmental change from an incomplete proxy record. *Quaternary Science Reviews, 265*, 107050.

Chase, B. M., & Meadows, M. E. (2007). Late Quaternary dynamics of Southern Africa's winter rainfall zone. *Earth-Science Reviews, 84*(3–4), 103–138.

Chase, B. M., & Quick, L. J. (2018). Influence of Agulhas forcing of Holocene climate change in South Africa's southern Cape. *Quaternary Research, 90*(2), 303–309.

Chase, B. M., Boom, A., Carr, A. S., Meadows, M. E., & Reimer, P. J. (2013). Holocene climate change in southernmost South Africa: Rock hyrax middens record shifts in the southern westerlies. *Quaternary Science Reviews, 82*, 199–205.

Chase, B. M., Boom, A., Carr, A. S., Carré, M., Chevalier, M., Meadows, M. E., Pedro, J. B., Stager, J. C., & Reimer, P. J. (2015a). Evolving southwest African response to abrupt deglacial North Atlantic climate change events. *Quaternary Science Reviews, 121*, 132–136.

Chase, B. M., Lim, S., Chevalier, M., Boom, A., Carr, A. S., Meadows, M. E., & Reimer, P. J. (2015b). Influence of tropical easterlies in Southern Africa's winter rainfall zone during the Holocene. *Quaternary Science Reviews, 107*, 138–148.

Chase, B. M., Chevalier, M., Boom, A., & Carr, A. S. (2017). The dynamic relationship between temperate and tropical circulation systems across South Africa since the last glacial maximum. *Quaternary Science Reviews, 174*, 54–62.

Chase, B. M., Harris, C., de Wit, M. J., Kramers, J., Doel, S., & Stankiewicz, J. (2021). South African speleothems reveal influence of high- and low-latitude forcing over the past 113.5 ky. *Geology, 49*(11), 1353–1357.

Chazan, M., Berna, F., Brink, J., Ecker, M., Holt, S., Porat, N., Lee-Thorp, J. A., & Horwitz, L. K. (2020). Archeology, environment, and chronology of the Early Middle Stone Age component of Wonderwerk Cave. *Journal of Paleolithic Archaeology, 3*, 302–335.

Clark, J. L. (2017). The Howieson's Poort fauna from Sibudu Cave: Documenting continuity and change within Middle Stone Age industries. *Journal of Human Evolution, 107*, 49–70.

Cleghorn, N., Potts, A. J., & Cawthra, H. C. (2020). The Palaeo-Agulhas Plain: A lost world and extinct ecosystem. *Quaternary Science Reviews, 235*, 106308.

Cockcroft, M. J., Wilkinson, M. J., & Tyson, P. D. (1987). The application of a present-day climatic model to the late Quaternary in Southern Africa. *Climatic Change, 10*(2), 161–181.

Codron, D., Codron, J., Lee-Thorp, J. A., Sponheimer, M., De Ruiter, D., Sealy, J., Grant, R., & Fourie, N. (2007). Diets of savanna ungulates from stable carbon isotope composition of faeces. *Journal of Zoology, 273*(1), 21–29.

Codron, D., Brink, J. S., Rossouw, L., Clauss, M., Codron, J., Lee-Thorp, J. A., & Sponheimer, M. (2008). Functional differentiation of African grazing ruminants: An example of specialized adaptations to very small changes in diet. *Biological Journal of the Linnean Society, 94*(4), 755–764.

Copeland, S. R., Cawthra, H. C., Fisher, E. C., Lee-Thorp, J. A., Cowling, R. M., Le Roux, P. J., Hodgkins, J., & Marean, C. W. (2016). Strontium isotope investigation of ungulate movement patterns on the Pleistocene Paleo-Agulhas Plain of the Greater Cape floristic region, South Africa. *Quaternary Science Reviews, 141*, 65–84.

Cordova, C. E. (2013). C3 Poaceae and Restionaceae phytoliths as potential proxies for reconstructing winter rainfall in South Africa. *Quaternary International, 287*, 121–140.

Cowling, R. M. (1983). The occurrence of C_3 and C_4 grasses in fynbos and allied shrublands in the South Eastern Cape, South Africa. *Oecologia, 58*(1), 121–127.

Cowling, R. M., & Holmes, P. M. (1992). Endemism and speciation in a lowland flora from the Cape Floristic Region. *Biological Journal of the Linnean Society, 47*(4), 367–383.

Cowling, R. M., Potts, A. J., Franklin, J., Midgley, G. F., Engelbrecht, F., & Marean, C. W. (2020). Describing a drowned Pleistocene ecosystem: Last Glacial Maximum vegetation reconstruction of the Palaeo-Agulhas Plain. *Quaternary Science Reviews, 235*, 105866.

Crimp, S. J., & Mason, S. J. (1999). The extreme precipitation event of 11 to 16 February 1996 over South Africa. *Meteorology and Atmospheric Physics, 70*(1–2), 29–42.

Deacon, H. J. (1983). Another look at the Pleistocene climates of South Africa. *South African Journal of Science, 79*(8), 325–328.

Deacon, J., & Lancaster, N. (1988). *Late Quaternary palaeoenvironments of Southern Africa* (p. 225). Clarendon Press.

Deacon, H. J., Deacon, J., Scholtz, A., Thackeray, J. F., Brink, J. S., & Vogel, J. C. (1984). Correlation of palaeoenvironmental data from the Late Pleistocene and Holocene deposits at Boomplaas Cave, southern Cape. In: Vogel, J. C. (ed.) *Late Cainozic palaeoclimates of the Southern Hemisphere. International symposium held by the South African Society for Quaternary Research; Swaziland.* Balkema, pp. 339–351.

Diamond, R. E., & Harris, C. (2019). Annual shifts in O- and H-isotope composition as measures of recharge: The case of the Table Mountain springs, Cape Town, South Africa. *Hydrogeology Journal, 27*(8), 2993–3008.

Diefendorf, A. F., Mueller, K. E., Wing, S. L., Koch, P. L., & Freeman, K. H. (2010). Global patterns in leaf ^{13}C discrimination and implications for studies of past and future climate. *Proceedings of the National Academy of Sciences, 107*(13), 5738–5743.

Dupont, L. M., & Kuhlmann, H. (2017). Glacial-interglacial vegetation change in the Zambezi catchment. *Quaternary Science Reviews, 155*, 127–135.

Dupont, L. M., Caley, T., Kim, J. H., Castañeda, I., Malaizé, B., & Giraudeau, J. (2011). Glacial-interglacial vegetation dynamics in South Eastern Africa coupled to sea surface temperature variations in the Western Indian Ocean. *Climate of the Past, 7*(4), 1209–1224.

Dupont, L. M., Zhao, X., Charles, C., Faith, J. T., & Braun, D. (2022). Continuous vegetation record of the Greater Cape Floristic Region (South Africa) covering the past 300 000 years (IODP U1479). *Climate of the Past, 18*(1), 1–21.

Ecker, M., Brink, J., Chazan, M., Horwitz, L. K., & Lee-Thorp, J. A. (2017). Radiocarbon dates constrain the timing of environmental and cultural shifts in the Holocene strata of Wonderwerk Cave, South Africa. *Radiocarbon, 59*(4), 1067–1086.

Ecker, M., Brink, J., Horwitz, L. K., Scott, L., & Lee-Thorp, J. A. (2018). A 12,000 year record of changes in herbivore niche separation and palaeoclimate (Wonderwerk Cave, South Africa). *Quaternary Science Reviews, 180*, 132–144.

Eckrich, C. A., Albeke, S. E., Flaherty, E. A., Bowyer, R. T., & Ben-David, M. (2020). rKIN: Kernel-based method for estimating isotopic niche size and overlap. *Journal of Animal Ecology, 89*(3), 757–771.

Engelbrecht, F. A., Marean, C. W., Cowling, R. M., Engelbrecht, C. J., Neumann, F. H., Scott, L., Nkoana, R., O'Neal, D., Fisher, E., Shook, E., Franklin, J., Thatcher, M., McGregor, J. L., Van der Merwe, J., Dedekind, Z., & Difford, M. (2019). Downscaling Last Glacial Maximum climate over Southern Africa. *Quaternary Science Reviews, 226*, 105879.

Esteban, I., Marean, C. W., Cowling, R. M., Fisher, E. C., Cabanes, D., & Albert, R. M. (2020a). Palaeoenvironments and plant availability during MIS 6 to MIS 3 on the edge of the Palaeo-Agulhas Plain (south coast, South Africa) as indicated by phytolith analysis at Pinnacle Point. *Quaternary Science Reviews, 235*, 105667.

Esteban, I., Bamford, M. K., House, A., Miller, C. S., Neumann, F. H., Schefuß, E., Pargeter, J., Cawthra, H. C., & Fisher, E. C. (2020b). Coastal palaeoenvironments and hunter-gatherer plant-use at Waterfall Bluff rock shelter in Mpondoland (South Africa) from MIS 3 to the Early Holocene. *Quaternary Science Reviews, 250*, 106664.

Faith, J. T. (2018). Paleodietary change and its implications for aridity indices derived from δ18O of herbivore tooth enamel. *Palaeogeography, Palaeoclimatology, Palaeoecology, 490*, 571–578.

Faith, J. T., Chase, B. M., & Avery, D. M. (2019). Late Quaternary micromammals and the precipitation history of the southern Cape, South Africa. *Quaternary Research, 91*(2), 848–860.

Fisher, E. C., Bar-Matthews, M., Jerardino, A., & Marean, C. W. (2010). Middle and Late Pleistocene paleoscape modeling along the southern coast of South Africa. *Quaternary Science Reviews, 29*(11–12), 1382–1398.

France, C. A., & Owsley, D. W. (2015). Stable carbon and oxygen isotope spacing between bone and tooth collagen and hydroxyapatite in human archaeological remains. *International Journal of Osteoarchaeology, 25*(3), 299–312.

Gagnon, M., & Chew, A. E. (2000). Dietary preferences in extant African Bovidae. *Journal of Mammalogy, 81*(2), 490–511.

Harris, C., Burgers, C., Miller, J., & Rawoot, F. (2010). O-and H-isotope record of Cape Town rainfall from 1996 to 2008, and its application to recharge studies of Table Mountain groundwater, South Africa. *South African Journal of Geology, 113*(1), 33–56.

Herbert, A. V., & Fitchett, J. M. (2022). Synthesising the pollen records for the Drakensberg-Maloti through quantitative modelling. *Quaternary International, 611*, 81–90.

Hermes, T. R., Frachetti, M. D., Bullion, E. A., Maksudov, F., Mustafokulov, S., & Makarewicz, C. A. (2018). Urban and nomadic isotopic niches reveal dietary connectivities along Central Asia's Silk Roads. *Scientific Reports, 8*(1), 5177.

Hette-Tronquart, N. (2019). Isotopic niche is not equal to trophic niche. *Ecology Letters, 22*(11), 1987–1989.

Hogg, A. G., Heaton, T. J., Hua, Q., Palmer, J. G., Turney, C. S., Southon, J., Bayliss, A., Blackwell, P. G., Boswijk, G., Ramsey, C. B., & Pearson, C. (2020). SHCal20 Southern Hemisphere calibration, 0–55,000 years cal BP. *Radiocarbon, 62*(4), 759–778.

Holmgren, K., Lee-Thorp, J. A., Cooper, G. R., Lundblad, K., Partridge, T. C., Scott, L., Sithaldeen, R., Talma, A. S., & Tyson, P. D. (2003). Persistent millennial-scale climatic variability over the past 25,000 years in Southern Africa. *Quaternary Science Reviews, 22*(21–22), 2311–2326.

Hublin, J. J., Ben-Ncer, A., Bailey, S. E., Freidline, S. E., Neubauer, S., Skinner, M. M., Bergmann, I., Cabec, A., Benazzi, S., Harvati, K., & Gunz, P. (2017). New fossils from Jebel Irhoud, Morocco and the pan-African origin of Homo sapiens. *Nature, 546*(7657), 289–292.

Hutchinson, G. E. (1957). Concluding remarks. *Cold Spring Harbor Symposia on Quantitative Biology, 22*, 415–427.

Ivanciu, I., Ndarana, T., Matthes, K., & Wahl, S. (2022). On the ridging of the South Atlantic Anticyclone over South Africa: The impact of Rossby wave breaking and of climate change. *Geophysical Research Letters, 49*(20), e2022GL099607.

Jackson, A. L., Inger, R., Parnell, A. C., & Bearhop, S. (2011). Comparing isotopic niche widths among and within communities: SIBER–Stable Isotope Bayesian Ellipses in R. *Journal of Animal Ecology, 80*(3), 595–602.

Jacobs, Z., & Roberts, R. G. (2009). Were environmental or demographic factors the driving force behind Middle Stone Age innovations in Southern Africa. *South African Journal of Science, 105*, 333–334.

Jacobs, Z., Roberts, R. G., Galbraith, R. F., Deacon, H. J., Grun, R., Mackay, A., Mitchell, P. J., Vogelsang, R., & Wadley, L. (2008a). Ages for the Middle Stone Age of Southern Africa: Implications for human behavior and dispersal. *Science, 322*, 733–735.

Jacobs, Z., Wintle, A., Duller, G., Roberts, R. G., & Wadley, L. (2008b). New ages for the post-Howiesons Poort, late and final Middle Stone Age at Sibudu, South Africa. *Journal of Archaeological Science, 35*, 1790–1807.

Jerardino, A. (1993). Mid-to late-Holocene sea-level fluctuations: The archaeological evidence at Tortoise Cave, South-western Cape, South Africa. *South African Journal of Science, 89*(10), 481–488.

Jerardino, A. (1995). Late Holocene Neoglacial episodes in southern South America and Southern Africa: A comparison. *The Holocene, 5*(3), 361–368.

Jerardino, A. (2022). Coastal foraging on the West Coast of South Africa in the midst of mid-Holocene climate change. *The Journal of Island and Coastal Archaeology, 17*(4), 585–605.

Jerardino, A., Navarro, R., Orton, J., Button, R., Halkett, D., Webley, L., Tusenius, M., Hoffman, T., & February, E. (2018). Late Holocene climatic and cultural variability at a focal point of settlement near Lamberts Bay, South Africa: Test excavations at Soutpansklipheuwel. *South African Archaeological Bulletin, 73*(207), 13–34.

Khumalo, W. (2022). *Using the fossil charcoal and pollen records from Elands Bay Cave and Boomplaas Cave, South Africa, to reconstruct variability in local hydroclimate and seasonality (Master's thesis*. University of Cape Town.

Kingdon, J. (1982). *East African mammals. Bovids*. University of Chicago Press.

Kingdon, J. (2015). *The Kingdon field guide to African mammals*. Bloomsbury Publishing.

Knight, J., & Fitchett, J. M. (2021). A proposed chronostratigraphic framework for the late Quaternary of Southern Africa. *South African Journal of Geology 2021, 124*(4), 843–862.

Knight, J., & Stratford, D. (2020). Investigating lithic scatters in arid environments: The Early and Middle Stone Age in Namibia. *Proceedings of the Geologists' Association, 131*(6), 778–783.

Kohn, M. J. (2010). Carbon isotope compositions of terrestrial C3 plants as indicators of (paleo)ecology and (paleo)climate. *Proceedings of the National Academy of Sciences, 107*(46), 19691–19695.

Lee-Thorp, J. A., & Beaumont, P. B. (1995). Vegetation and seasonality shifts during the late Quaternary deduced from 13C/12C ratios of grazers at Equus Cave, South Africa. *Quaternary Research, 43*(3), 426–432.

Lehmann, S. B., Levin, N. E., Braun, D. R., Stynder, D. D., Zhu, M., Le Roux, P. J., & Sealy, J. (2018). Environmental and ecological implications of strontium isotope ratios in mid-Pleistocene fossil teeth from Elandsfontein, South Africa. *Palaeogeography, Palaeoclimatology, Palaeoecology, 490*, 84–94.

Levin, N. E., Cerling, T. E., Passey, B. H., Harris, J. M., & Ehleringer, J. R. (2006). A stable isotope aridity index for terrestrial environments. *Proceedings of the National Academy of Sciences, 103*(30), 11201–11205.

Levin, N. E., Zipser, E. J., & Cerling, T. E. (2009). Isotopic composition of waters from Ethiopia and Kenya: Insights into moisture sources for eastern Africa. *Journal of Geophysical Research, 114*(D23), D23.

Levin, N. E., Haile-Selassie, Y., Frost, S. R., & Saylor, B. Z. (2015). Dietary change among hominins and cercopithecids in Ethiopia during the early Pliocene. *Proceedings of the National Academy of Sciences, 112*(40), 12304–12309.

Loftus, E., Stewart, B. A., Dewar, G., & Lee-Thorp, J. A. (2015). Stable isotope evidence of late MIS 3 to middle Holocene palaeoenvironments from Sehonghong Rockshelter, eastern Lesotho. *Journal of Quaternary Science, 30*(8), 805–816.

Loftus, E., Sealy, J., & Lee-Thorp, J. A. (2016). New radiocarbon dates and Bayesian models for Nelson Bay Cave and Byneskranskop 1: Implications for the South African Later Stone Age sequence. *Radiocarbon, 58*(2), 365–381.

Loftus, E., Pargeter, J., Mackay, A., Stewart, B. A., & Mitchell, P. J. (2019). Late Pleistocene human occupation in the Maloti-Drakensberg region of Southern Africa: New radiocarbon dates from Rose Cottage Cave and inter-site comparisons. *Journal of Anthropological Archaeology, 56*, 101117.

Lombard, M., Bradfield, J., Caruana, M. V., Makhubela, T. V., Dusseldorp, G. L., Kramers, J. D., & Wurz, S. (2022). The Southern African Stone Age sequence updated (II). *South African Archaeological Bulletin, 77*(217), 172–212.

Lüdecke, T., Leichliter, J. N., Aldeias, V., Bamford, M. K., Biro, D., Braun, D. R., Capelli, C., Cybulski, J. D., Duprey, N. N., Ferreira da Silva, M. J., Foreman, A. D., Habermann, J. M., Haug, G. H.,

Martinez, F. I., Mathe, J., Mulch, A., Sigman, D. M., Vonhof, H., Bobe, R., … Martínez-García, A. (2022). Carbon, nitrogen, and oxygen stable isotopes in modern tooth enamel: A case study from Gorongosa National Park, Central Mozambique. *Frontiers in Ecology and Evolution, 10*, 1107.

Lukich, V., Cowling, S., & Chazan, M. (2020). Palaeoenvironmental reconstruction of Kathu Pan, South Africa, based on sedimentological data. *Quaternary Science Reviews, 230*, 106153.

Luyt, J., Hare, V. J., & Sealy, J. (2019). The relationship of ungulate $\delta^{13}C$ and environment in the temperate biome of Southern Africa, and its palaeoclimatic application. *Palaeogeography, Palaeoclimatology, Palaeoecology, 514*, 282–291.

Mackay, A., Stewart, B. A., & Chase, B. M. (2014). Coalescence and fragmentation in the late Pleistocene archaeology of southernmost Africa. *Journal of Human Evolution, 72*, 26–51.

Mackay, A., Armitage, S. J., Niespolo, E. M., Sharp, W. D., Stahlschmidt, M. C., Blackwood, A. F., Boyd, K. C., Chase, B. M., Lagle, S. E., Kaplan, C. F., Low, M. A., Martisius, N. L., McNeill, P. J., Moffat, I., O'Driscoll, C. A., Rudd, R., Orton, J., & Steele, T. E. (2022). Environmental influences on human innovation and behavioural diversity in Southern Africa 92–80 thousand years ago. *Nature Ecology & Evolution, 6*(4), 361–369.

Marean, C. W., Cowling, R. M., & Franklin, J. (2020). The Palaeo-Agulhas Plain: Temporal and spatial variation in an extraordinary extinct ecosystem of the Pleistocene of the Cape Floristic Region. *Quaternary Science Reviews, 235*, 106161.

McCall, G. S. (2007). Behavioral ecological models of lithic technological change during the later Middle Stone Age of South Africa. *Journal of Archaeological Science, 34*(10), 1738–1751.

Miller, G. H., Beaumont, P. B., Deacon, H. J., Brooks, A. S., Hare, P. E., & Jull, A. J. T. (1999). Earliest modern humans in Southern Africa dated by isoleucine epimerization in ostrich eggshell. *Quaternary Science Reviews, 18*(13), 1537–1548.

Mitchell, P. J. (1993a). Archaeological investigations at two Lesotho rock-shelters: Terminal Pleistocene/early Holocene assemblages from Ha Makotoko and Ntloana Tsoana. *Proceedings of the Prehistoric Society, 59*, 39–60.

Mitchell, P. J. (1993b). The archaeology of Tloutle rock shelter, Maseru District, Lesotho. *Navorsinge van die Nasionale Museum: Researches of the National Museum, 9*(4), 78–79.

Mitchell, P. J., & Vogel, J. C. (1994). New radiocarbon dates from Sehonghong rock shelter, Lesotho. *South African Journal of Science, 90*(5), 284–288.

Mucina, L., & Rutherford, M. C. (2006). *The vegetation of South Africa, Lesotho and Swaziland*. Pretoria: South African National Biodiversity Institute.

Nel, T. H., & Henshilwood, C. S. (2016). The small mammal sequence from the c. 76–72 ya Still Bay levels at Blombos Cave, South Africa–taphonomic and palaeoecological implications for human behaviour. *PLoS ONE, 11*(8), e0159817.

Newsome, S. D., Martinez del Rio, C., Bearhop, S., & Phillips, D. L. (2007). A niche for isotopic ecology. *Frontiers in Ecology and the Environment, 5*(8), 429–436.

Pargeter, J., Loftus, E., & Mitchell, P. J. (2017). New ages from Sehonghong rock shelter: Implications for the late Pleistocene occupation of highland Lesotho. *Journal of Archaeological Science: Reports, 12*, 307–315.

Pargeter, J., Loftus, E., Mackay, A., Mitchell, P. J., & Stewart, B. (2018). New ages from Boomplaas Cave, South Africa, provide increased resolution on late/terminal Pleistocene human behavioural variability. *Azania: Archaeological Research in Africa, 53*(2), 156–184.

Parker, A. G., Lee-Thorp, J., & Mitchell, P. J. (2011). Late Holocene Neoglacial conditions from the Lesotho highlands, Southern Africa: Phytolith and stable carbon isotope evidence from the archaeological site of Likoaeng. *Proceedings of the Geologists' Association, 122*(1), 201–211.

Pestle, W. J., Crowley, B. E., & Weirauch, M. T. (2014). Quantifying inter-laboratory variability in stable isotope analysis of ancient skeletal remains. *PLoS ONE, 9*(7), e102844.

Phillipson, D. W. (1973). The prehistoric succession in Eastern Zambia: A preliminary report. *Azania, 8*, 3–24.

Phillipson, D. W. (1976). *The prehistory of eastern Zambia*. Nairobi, Kenya: British Institute in Eastern Africa.

Preston-Whyte, R. A., & Tyson, P. D. (1988). *Atmosphere and weather of Southern Africa*. Oxford University Press.

Quick, L. J., Meadows, M. E., Bateman, M. D., Kirsten, K. L., Mäusbacher, R., Haberzettl, T., & Chase, B. M. (2016). Vegetation and climate dynamics during the last glacial period in the fynbos-afrotemperate forest ecotone, southern Cape, South Africa. *Quaternary International, 404*, 136–149.

Rebelo, A. G., Boucher, C., Helme, N., Mucina, L., Rutherford, M. C. (2006). Fynbos biome. In: Mucina, L., & Rutherford, M. C. (eds.), *The vegetation of South Africa, Lesotho and Swaziland,* Pretoria: South African National Biodiversity Institute, pp. 52–219.

Reynard, J. P. (2021). Paradise lost: Large mammal remains as a proxy for environmental change from MIS 6 to the Holocene in Southern Africa. *South African Journal of Geology 2021, 124*(4), 1055–1072.

Rhodes, S. E., Goldberg, P., Ecker, M., Horwitz, L. K., Boaretto, E., & Chazan, M. (2022). Exploring the Later Stone Age at a micro-scale: New high-resolution excavations at Wonderwerk Cave. *Quaternary International, 614*, 126–145.

Roberts, P., Lee-Thorp, J. A., Mitchell, P. J., & Arthur, C. (2013). Stable carbon isotopic evidence for climate change across the late Pleistocene to early Holocene from Lesotho, Southern Africa. *Journal of Quaternary Science, 28*(4), 360–369.

Roberts, P., Fernandes, R., Craig, O. E., Larsen, T., Lucquin, A., Swift, J., & Zech, J. (2018). Calling all archaeologists: Guidelines for terminology, methodology, data handling, and reporting when undertaking and reviewing stable isotope applications in archaeology. *Rapid Communications in Mass Spectrometry, 32*(5), 361–372.

Robinson, J. R. (2017). Thinking locally: Environmental reconstruction of Middle and Later Stone Age archaeological sites in Ethiopia, Kenya, and Zambia based on ungulate stable isotopes. *Journal of Human Evolution, 106*, 19–37.

Robinson, J. R. (2022). Investigating isotopic niche space: Using rKIN for stable isotope studies in archaeology. *Journal of Archaeological Method and Theory, 29*(3), 831–861.

Robinson, J. R., & Rowan, J. (2017). Holocene paleoenvironmental change in Southeastern Africa (Makwe Rockshelter, Zambia): Implications for the spread of pastoralism. *Quaternary Science Reviews, 156*, 57–68.

Robinson, J. R., & Wadley, L. (2018). Stable isotope evidence for (mostly) stable local environments during the South African Middle Stone Age from Sibudu, KwaZulu-Natal. *Journal of Archaeological Science, 100*, 32–44.

Roffe, S. J., Fitchett, J. M., & Curtis, C. J. (2021). Investigating changes in rainfall seasonality across South Africa: 1987–2016. *International Journal of Climatology, 41*, E2031–E2050.

Scerri, E. M., Thomas, M. G., Manica, A., Gunz, P., Stock, J. T., Stringer, C., Grove, M., Groucutt, H. S., Timmermann, A., Rightmire, G. P., & d'Errico, F. (2018). Did our species evolve in subdivided populations across Africa, and why does it matter? *Trends in Ecology & Evolution, 33*(8), 582–594.

Scerri, E. M., Chikhi, L., & Thomas, M. G. (2019). Beyond multiregional and simple out-of-Africa models of human evolution. *Nature Ecology & Evolution, 3*(10), 1370–1372.

Schoville, B. J., Brown, K. S., & Wilkins, J. (2022). A lithic provisioning model as a proxy for landscape mobility in the Southern and Middle Kalahari. *Journal of Archaeological Method and Theory, 29*(1), 162–187.

Scott, L. (1989). Climatic conditions in Southern Africa since the last glacial maximum, inferred from pollen analysis. *Palaeogeography, Palaeoclimatology, Palaeoecology, 70*(4), 345–353.

Scott, L., & Nyakale, M. (2002). Pollen indications of Holocene palaeoenvironments at Florisbad spring in the central Free State, South Africa. *The Holocene, 12*(4), 497–503.

Scott, L., Holmgren, K., Talma, A. S., Woodborne, S., & Vogel, J. C. (2003). Age interpretation of the Wonderkrater spring sediments and vegetation change in the Savanna Biome, Limpopo Province, South Africa. *South African Journal of Science, 99*(9), 484–488.

Sealy, J. (2016). Cultural change, demography, and the archaeology of the last 100 kyr in Southern Africa. In S. Jones & B. Stewart (Eds.), *Africa from MIS 6–2* (pp. 65–75). Springer.

Sealy, J., Lee-Thorp, J., Loftus, E., Faith, J. T., & Marean, C. W. (2016). Late Quaternary environmental change in the southern Cape, South Africa, from stable carbon and oxygen isotopes in faunal tooth enamel from Boomplaas Cave. *Journal of Quaternary Science, 31*(8), 919–927.

Sealy, J., Naidoo, N., Hare, V. J., Brunton, S., & Faith, J. T. (2020). Climate and ecology of the palaeo-Agulhas Plain from stable carbon and oxygen isotopes in bovid tooth enamel from Nelson Bay Cave, South Africa. *Quaternary Science Reviews, 235*, 105974.

Skinner, J. D., & Chimimba, C. T. (2005). *The mammals of the Southern African sub-region*. Cambridge University Press.

Smith, J. M., Lee-Thorp, J. A., & Sealy, J. C. (2002). Stable carbon and oxygen isotopic evidence for late Pleistocene to middle Holocene climatic fluctuations in the interior of Southern Africa. *Journal of Quaternary Science: Published for the Quaternary Research Association, 17*(7), 683–695.

Sponheimer, M., Lee-Thorp, J. A., DeRuiter, D. J., Smith, J. M., Van Der Merwe, N. J., Reed, K., Grant, C. C., Ayliffe, L. K., Robinson, T. F., Heidelberger, C., & Marcus, W. (2003). Diets of Southern African Bovidae: Stable isotope evidence. *Journal of Mammalogy, 84*(2), 471–479.

Stewart, B. A., & Mitchell, P. J. (2018). Late Quaternary palaeoclimates and human-environment dynamics of the Maloti-Drakensberg region, Southern Africa. *Quaternary Science Reviews, 196*, 1–20.

Stewart, B. A., Zhao, Y., Mitchell, P. J., Dewar, G., Gleason, J. D., & Blum, J. D. (2020). Ostrich eggshell bead strontium isotopes reveal persistent macroscale social networking across late Quaternary Southern Africa. *Proceedings of the National Academy of Sciences, 117*(12), 6453–6462.

Stowe, M. J., & Sealy, J. (2016). Terminal Pleistocene and Holocene dynamics of Southern Africa's winter rainfall zone based on carbon and oxygen isotope analysis of bovid tooth enamel from Elands Bay Cave. *Quaternary International, 404*, 57–67.

Stratford, D., Braun, K., & Morrissey, P. (2021). Cave and rock shelter sediments of Southern Africa: A review of the chronostratigraphic and palaeoenvironmental record from Marine Isotope Stage 6 to 1. *South African Journal of Geology, 124*(4), 879–914.

Strobel, P., Bliedtner, M., Carr, A. S., Struck, J., du Plessis, N., Glaser, B., Meadows, M. E., Quick, L. J., Zech, M., Zech, R., & Haberzettl, T. (2022). Reconstructing Late Quaternary precipitation and its source on the southern Cape coast of South Africa: A multi-proxy paleoenvironmental record from Vankervelsvlei. *Quaternary Science Reviews, 284*, 107467.

Talma, A. S., & Vogel, J. C. (1992). Late Quaternary paleotemperatures derived from a speleothem from Cango Caves, Cape Province, South Africa. *Quaternary Research, 37*(2), 203–213.

Thomas, D. S., & Burrough, S. L. (2012). Interpreting geoproxies of late Quaternary climate change in African drylands: Implications for understanding environmental change and early human behaviour. *Quaternary International, 253*, 5–17.

Thomas, D. S., & Burrough, S. L. (2016). Luminescence-based dune chronologies in Southern Africa: Analysis and interpretation of dune database records across the subcontinent. *Quaternary International, 410*, 30–45.

Tyson, P. D., & Preston-Whyte, R. A. (2000). *Weather and climate of Southern Africa*. Oxford University Press.

Val, A., & Collins, B. (2022). From veld to coast: Towards an understanding of the diverse landscapes' uses by past foragers in Southern Africa. *Journal of Paleolithic Archaeology, 5*(1), 16.

Van Zinderen Bakker, E. M. (1967). Upper Pleistocene stratigraphy and Holocene ecology on the basis of vegetation changes in Sub-Saharan Africa. In W. W. Bishop & J. D. Clark (Eds.), *Background to evolution in Africa* (pp. 125–147). University of Chicago Press.

Van Zinderen Bakker, E. M. (1976). Evolution of Late Quaternary palaeoclimates of Southern Africa. *Palaeoecology of Africa & of the Surrounding Islands & Antarctica, 9*, 160–202.

Vogel, J. C. (1978). The geographical distribution of Kranz species in Southern Africa. *South African Journal of Science, 75*, 209–215.

Vogel, J. C. (1983). Isotopic evidence for the past climates and vegetation of Southern Africa. *Bothalia, 14*(3/4), 391–394.

Vogel, J. C. (2001). Radiometric dates for the Middle Stone Age in South Africa. In P. V. Tobias (Ed.), *Humanity from African naissance to coming millenia: Colloquia in human biology and palaeoanthropology* (pp. 261–268). Firenze University Press.

Wadley, L. (1995). Review of dated Stone Age sites recently excavated in the eastern Free State, South Africa. *South African Journal of Science, 91*(11–12), 574–579.

Wadley, L. (1997). Rose Cottage Cave: Archaeological work 1987 to 1997. *South African Journal of Science, 93*(10), 439–444.

Wadley, L. (2001). What is cultural modernity? A general view and a South African perspective from Rose Cottage Cave. *Cambridge Archaeological Journal, 11*(2), 201–221.

Wadley, L. (2015). Those marvellous millennia: The Middle Stone Age of Southern Africa. *Azania: Archaeological Research in Africa, 50*(2), 155–226.

Wadley, L. (1991). Rose Cottage Cave: Background and a preliminary report on the recent excavations. *The South African Archaeological Bulletin, 46*, 125–130.

Wadley, L. (1996). The Robberg Industry of Rose Cottage Cave, eastern Free State: The technology, spatial patterns and environment. *The South African Archaeological Bulletin, 51*, 64–74.

Wadley, L. (2000). The early Holocene layers of Rose Cottage Cave, eastern Free State: Technology, spatial patterns and environment. *The South African Archaeological Bulletin, 55*, 18–31.

Wang, Y. V., Larsen, T., Leduc, G., Andersen, N., Blanz, T., & Schneider, R. R. (2013). What does leaf wax δD from a mixed C_3/C_4 vegetation region tell us? *Geochimica et Cosmochimica Acta, 111*, 128–139.

Ward, I., Bastos, A., Carabias, D., Cawthra, H., Farr, H., Green, A., & Sturt, F. (2022). Submerged palaeolandscapes of the Southern Hemisphere (SPLOSH) – What is emerging from the Southern Hemisphere. *World Archaeology, 54*(1), 6–28.

Way, A. M., de la Peña, P., de la Peña, E., & Wadley, L. (2022). Howiesons Poort backed artifacts provide evidence for social connectivity across Southern Africa during the Final Pleistocene. *Scientific Reports, 12*(1), 1–12.

West, A. G., February, E. C., & Bowen, G. J. (2014). Spatial analysis of hydrogen and oxygen stable isotopes ("isoscapes") in ground water and tap water across South Africa. *Journal of Geochemical Exploration, 145*, 213–222.

White, F. (1983). *The Vegetation of Africa, a Descriptive Memoir to Accompany the UNESCO/AETFAT/UNSO Vegetation Map of Africa*. Paris: UNESCO.

Wilkins, J. (2021). *Homo sapiens* origins and evolution in the Kalahari Basin, Southern Africa. *Evolutionary Anthropology: Issues, News, and Reviews, 30*(5), 327–344.

Yandel, A. W., Bolus, M., Bretzke, K., Bruch, A. A., Haidle, M. N., Hertler, C., & Märker, M. (2016). Increasing behavioral flexibility? An integrative macro-scale approach to understanding the Middle Stone Age of Southern Africa. *Journal of Archaeological Method and Theory, 23*(2), 623–668.

Ziegler, M., Simon, M. H., Hall, I. R., Barker, S., Stringer, C., & Zahn, R. (2013). Development of Middle Stone Age innovation linked to rapid climate change. *Nature Communications, 4*(1), 1–9.